



1 **Impacts of Tibetan Plateau uplift on atmospheric dynamics**
2 **and associated precipitation $\delta^{18}\text{O}$**

3

4 **S. Botsyun¹, P. Sepulchre¹, C. Risi², and Y. Donnadieu¹**

5 [1]{Laboratoire des Sciences du Climat et de l'Environnement, LSCE/IPSL, CEA-CNRS-
6 UVSQ, Université Paris-Saclay, Gif-sur-Yvette, France}

7 [2]{Laboratoire de Météorologie Dynamique, LMD/IPSL, UPMC, CNRS, Paris, France}

8 Correspondence to: S. Botsyun (svetlana.botsyun@lsce.ipsl.fr)

9

10 **Abstract**

11 Paleoelevation reconstructions of mountain belts have become a focus of modern science
12 since surface elevation provides crucial information for understanding both geodynamic
13 mechanisms of Earth's interior and influence of mountains growth on climate. Stable oxygen
14 isotopes paleoaltimetry is one of the most popular techniques nowadays, and relies on the
15 difference between $\delta^{18}\text{O}$ of paleo-precipitation reconstructed using the natural archives, and
16 modern measured values for the point of interest. Our goal is to understand where and how
17 complex climatic changes linked with the growth of mountains affect $\delta^{18}\text{O}$ in precipitation.
18 For this purpose, we develop a theoretical expression for the precipitation composition and we
19 use the isotope-equipped atmospheric general circulation model LMDZ-iso. Experiments with
20 reduced height over the Tibetan Plateau and the Himalayas have been designed. Our results
21 show that the isotopic composition of precipitation is very sensitive to climate changes related
22 with the growth of the Himalayas and Tibetan Plateau, notably changes in relative humidity
23 and precipitation amount. The relative contribution of controlling factors and their magnitude
24 differ depending on the uplift stage and the region considered. Thus future paleoaltimetry
25 studies should take into account constraints on climatic factors to avoid misestimating ancient
26 altitudes.

27



1 1 Introduction

2 Despite ongoing debates regarding the thermal and mechanical nature of mechanisms
3 involved (Boos, 2015; Chen et al., 2014), the Himalayas and the Tibetan Plateau (hereafter
4 TP) have long been considered to exert major influences on Asian atmospheric dynamics,
5 notably by reinforcing South Asian monsoon and driving subsidence ultimately leading to
6 onsets of deserts over Central Asia (Rodwell and Hoskins, 2001; Broccoli and Manabe,
7 1992). Thus, reconstructing the history of Himalayas and TP uplift appears crucial to
8 understand long-term climate evolution of Asia. On the other hand, topography uplift of TP is
9 ultimately driven by collision between India and Asia continents (Molnar et al., 2010),
10 making the timing and scale of surface elevation growth widely used for reconstructing the
11 rate and style of this tectonic plates convergence (eg. Royden et al., 2008; Tapponnier et al.,
12 2001).

13 Elevation reconstructions for the Tibetan Plateau and Himalayas are based on fossil-leaf
14 morphologies (eg. Antal, 1993; Forest et al., 1999; Khan et al., 2014), pollen (Dupont-Nivet
15 et al., 2008) correlation between stomatal density and the decrease in CO₂ partial pressure
16 with altitude (McElwain, 2004) and carbonate oxygen isotopic compositions (Currie et al.,
17 2005; DeCelles et al., 2007; Garzzone et al., 2000; Polissar et al., 2009; Rowley and Currie,
18 2006; Saylor et al., 2009; Xu et al., 2013; Zhuang et al., 2014; Li et al., 2015). In contrast to
19 paleobotanical methods, oxygen isotope paleoaltimetry has been widely applied for the
20 Cenozoic. Carbonate $\delta^{18}\text{O}$ is related to topography change using $\delta^{18}\text{O}$ -elevation relationship.
21 These relationships have been calibrated both empirically (eg. Garzzone et al., 2000; Poage
22 and Chamberlain, 2001) and theoretically, using basic thermodynamic principles, including
23 Rayleigh distillation, that govern isotopic fractionation processes (Rowley and Garzzone,
24 2007; Rowley et al., 2001).

25 The difference between paleoprecipitation $\delta^{18}\text{O}$ detected from natural archives and modern
26 values of the site of interest is identified with the effect of the surface uplift in numerous
27 recent studies (Currie et al., 2005; Cyr et al., 2005; Ding et al., 2014; Hoke et al., 2014;
28 Mulch, 2016; Rowley and Currie, 2006; Rowley et al., 2001; Xu et al., 2013). In the absence
29 of direct measurements of “paleo” altitude- $\delta^{18}\text{O}$ relationship *in situ*, stable-isotope
30 paleoaltimetry is potentially hampered by the fact that the presumed constancy of altitude-
31 $\delta^{18}\text{O}$ relationships through time might not be valid. For instance for the Andes, not
32 considering the impact of uplift on climate dynamics and related $\delta^{18}\text{O}$ values has been shown



1 to produce errors in paleoelevation reconstruction reaching up to $\pm 50\%$ (Ehlers and Poulsen,
2 2009; Poulsen et al., 2010). Regional climate variables and associated isotopic signal in
3 precipitation can also be affected by global climate change (Jeffery et al., 2012; Poulsen and
4 Jeffery, 2011). Moreover, it has been suggested that climate-driven changes in surface ocean
5 $\delta^{18}\text{O}$ through the Cenozoic can also influence recorded values of precipitation $\delta^{18}\text{O}$ over the
6 continent (Ding et al., 2014). Over TP, mismatches between paleoelevation estimations from
7 palynological and stable isotope data (eg. Sun et al., 2014) could be related to complex
8 climatic changes and associated variations of altitude- $\delta^{18}\text{O}$ relationship linked to the uplift,
9 still a detailed assessment of the consequences of topographic changes on precipitation $\delta^{18}\text{O}$ is
10 lacking.

11 Spatial distribution of isotopes in precipitation was described using various types of models,
12 from one-dimensional to three-dimensional general circulation (Craig, 1961; Dansgaard,
13 1964; Gedzelman and Arnold, 1994; Risi et al., 2010; Stowhas and Moyano, 1993). Such
14 modelling studies show how large-scale Asian monsoon circulation influence precipitation
15 $\delta^{18}\text{O}$ (He et al., 2015; LeGrande and Schmidt, 2009; Pausata et al., 2011; Vuille et al., 2005).
16 At the global scale, precipitation $\delta^{18}\text{O}$ has been shown to be affected by several factors other
17 than elevation, including mixing between air masses (Ehlers and Poulsen, 2009; Gat, 1996),
18 large-scale subsidence (e.g. Frankenberg et al., 2009), continental recycling (Lee et al., 2012;
19 Risi et al., 2013), deep convection (Risi et al., 2008), and enrichments linked to global
20 warming (Poulsen and Jeffery, 2011). Numerous studies have investigated the impact of
21 Asian topography on climate change, including the monsoon intensification (ex. Harris, 2006;
22 Kutzbach et al., 1989; Raymo and Ruddiman, 1992; Zhang et al., 2015; Zhisheng et al., 2015)
23 and Asian interior aridification onset (Broccoli and Manabe, 1992; Liu et al., 2015).
24 Nonetheless the linkage between these “climatic parameters” altered by the growth of TP and
25 their influence on the isotopic signal remain unclear. In this article we use numerical
26 modelling to provide some insights.

27

28 **2 Methods**

29 **2.1 Model simulations**

30 We use an Atmospheric General Circulation model (GCM) developed at Laboratoire de
31 Météorologie Dynamique, Paris, France with isotopes-tracking implement, called LMDZ-iso



1 (Risi et al., 2010). LMDZ-iso is derived from the LMDz model (Hourdin et al., 2006) that has
2 been used for numerous future and paleoclimate studies (Ladant et al., 2014; Pohl et al., 2014;
3 Sepulchre et al., 2006). Water in a condensed form and its vapour are advected by the Van
4 Leer advection scheme (Van Leer, 1977). Isotopic processes in LMDZ-iso are documented in
5 (Risi et al., 2010). Evaporation over land is assumed not to fractionate, given the simplicity of
6 the model surface parameterisation (Risi et al., 2010). Yao et al. (2013) have provided a
7 precise description of rainfall patterns over the TP, and showed LMDZ-iso ability to simulate
8 atmospheric dynamics and reproduce rainfall and $\delta^{18}\text{O}$ patterns consistent with data over this
9 region.

10 LMDZ-iso is also equipped with water tagging capabilities, allowing to quantify different
11 moisture contributions from continental and oceanic evaporation sources. The advantage of
12 this technique compared to typical back-trajectories methods is that it tracks the water rather
13 than air masses, thus taking into account effects of phase changes. In our simulations five
14 potential moisture sources are considered: (1) continental sources, (2) Indian Ocean, (3)
15 Atlantic Ocean, (4) Mediterranean Sea, and (5) Pacific Ocean.

16 We use a model configuration with 96 grid points in longitude, 72 in latitude and 19 vertical
17 layers, with the first four layers in the first kilometer above the surface. LMDZ-iso has a
18 stretchable grid that allows increased spatial resolution over a defined region. In our case, it
19 gives an averaged resolution of ~ 100 km over central Asia, which is a good trade-off between
20 a reasonable computing time and a spatial resolution that adequately represents main features
21 of TP topography.

22 Here we report results from three experiments designed to isolate the influence of Asian
23 topography on climate and isotopic composition of precipitation. Topography is derived from
24 a 10-minute US Navy dataset and interpolated to the model grid. The control run (MOD) is a
25 pre-industrial run, i.e. initialized with boundary conditions (insolation, greenhouse gases, sea
26 surface temperatures (SSTs), topography) kept at pre-industrial values. For the two other
27 experiments, we keep all boundary conditions (including albedo, rugosity, and vegetation
28 distribution) similar to those in MOD run, except for the topography. We reduce the altitude
29 over the area covering the Tibetan Plateau, Himalayas and a part of surrounding mountains:
30 Tian Shan, Pamir, Kunlun and Hindu Kush to 50% of modern elevations (intermediate, INT
31 case) and to 250-m elevation (low, LOW case) (Fig. 1). SSTs for all runs come from the
32 AMIP dataset (monthly SSTs averaged from 1979 to 1996; Taylor et al., 2000). Each



1 experiment has been run for 20 years. We analyse seasonal means over the last 18 years, as
 2 the two first years are extracted for spin-up.

3 **2.2 Theoretical framework for the precipitation composition**

4 Our goal is to understand to what extent topography changes explain the precipitation $\delta^{18}\text{O}$
 5 signal over TP (i.e. the direct topography effect) and what part of this signal depends on other
 6 climate processes. To do so, we develop a theoretical expression for the precipitation
 7 composition.

8 To the first order, the $\delta^{18}\text{O}$ composition of the precipitation R_p follows that of the vapour R_v .
 9 Deviations from the vapour composition, $\varepsilon = R_p - R_v$, are associated with local condensational
 10 or post condensational process.

$$11 \quad R_p = R_v + \varepsilon \quad (1)$$

12 In an idealized framework of an isolated air parcel transported from an initial site at low
 13 altitude to the site of interest (Fig. 2), the vapour composition can be predicted by Rayleigh
 14 distillation:

$$15 \quad R_v = R_{vi} \cdot f^{(\alpha-1)} \quad (2)$$

16 where R_{vi} is the initial composition of the vapour at the initial site, α is the fractionation
 17 coefficient, that depends on temperature and on the water phase (Majzoub, 1971; Merlivat
 18 and Nief, 1967), and f is the residual fraction of the vapour at the site of interest relatively to
 19 the initial site. We take the initial site as characterised by a temperature and humidity T_0 and
 20 q_0 . Under these conditions, we note R_{v0} the theoretic isotopic composition that it would have
 21 if all the vapour originated from the local evaporation over quiescent oceanic conditions.
 22 Depending on the atmospheric circulation, on deep convective and mixing processes and on
 23 the site of interest, the initial site may be characterised by a different isotopic composition:

$$24 \quad R_{vi} = R_{v0} + \delta R_{vi} \quad (3)$$

25 The residual fraction f depends on the minimum condensation temperature that the parcel has
 26 undergone along its trajectory towards the site of interest, T^* (Galewsky and Hurley, 2010;
 27 Galewsky et al., 2005; Sherwood, 1996):

$$28 \quad f = q_s(T^*)/q_0 \quad (4)$$

29 where q_s is the saturation specific humidity, function of temperature following the Clausius-
 30 Clapeyron relationship.



1 If we assume that the air at the site of interest has been transported adiabatically from the area
 2 of minimum condensation temperature, then:

$$3 \quad q_s(T^*) = h \cdot q_s(T_s) \quad (5)$$

4 when h and T_s are the relative humidity and air temperature near the surface of the site of
 5 interest.

6 The surface temperature can be predicted to the first order by the adiabatic lapse rate, Γ , and
 7 is modulated by the non-adiabatic component, δT_s that represents processes such as large-
 8 scale circulation or radiation:

$$9 \quad T_s = T_0 + \Gamma \cdot (z - z_0) + \delta T_s \quad (6)$$

10 where z and z_0 are the altitudes at the site of interest and at the initial site. We use an adiabatic
 11 lapse rate equal to 5° km^{-1} based on the measurements of modern observed mean temperature
 12 lapse rate on the southern slope of the central Himalayas, that ranges from 4.7 to $6.1^\circ \text{ km}^{-1}$
 13 for the monsoon season and from 4.3 to $5.5^\circ \text{ km}^{-1}$ for the rest of the year (Kattal et al., 2015).

14 If we combine Eq. (1) to Eq. (6), we get that R_v is a function of δR_{vi} , ε , h , δT_s and z :

$$15 \quad R_p = R_p(\delta R_{vi}, \varepsilon, h, \delta T_s, z) \quad (7)$$

16 Parameters z_0 , q_0 , T_0 are reference values that are common to all sites of interest, all climates
 17 and geographies. Even if initial conditions for the Rayleigh distillation vary depending on the
 18 atmosphere circulation, on deep convective processes and on the site of interest, we keep the
 19 same reference values and we consider all variations in initial conditions are accommodated
 20 by δR_{vi} .

21 This model is equivalent to that of Rowley et al. (2001) for $\delta R_{vi} = 0$ (i.e. neglecting the effects
 22 of mixing and deep convection on the initial water vapour), $\varepsilon = (\alpha - 1) \cdot R_v$ (i.e. neglecting
 23 post-condensational effects), and $h = 1$ (i.e. assuming the site of interest is inside the
 24 precipitating cloud).

25 **2.3 Decomposing precipitation composition differences**

26 Our goal is to understand why R_p varies from one climatic state to another. Let's refer to these
 27 climatic states using subscript 1 and 2 and to their difference using the Δ notation.
 28 Differences between INT and LOW and between MOD and INT climatic states corresponds
 29 to the initial and the terminate stages of the TP uplift respectively. We decompose $\Delta R_p = R_{p2} -$
 30 R_{p1} into contribution from $\Delta \delta R_{vi}$, $\Delta \varepsilon$, Δh , $\Delta \delta T_s$, and Δz :



$$\Delta R_p = \frac{\partial R_p}{\partial R_{vi}} \cdot \Delta \delta R_{vi} + \frac{\partial R_p}{\partial \varepsilon} \cdot \Delta \varepsilon + \frac{\partial R_p}{\partial h} \cdot \Delta h + \frac{\partial R_p}{\partial \delta T_s} \cdot \Delta \delta T_s + \frac{\partial R_p}{\partial z} \cdot \Delta z \quad (8)$$

To estimate each of these terms, we estimate difference between R_p calculated from the different values of δR_{vi} , ε , h , δT_s , and z , changing only one parameter at a time, as detailed in table 1 (and see next section). Our method to estimate the terms in Eq. (8) is equivalent to first order approximation of partial derivatives, i.e. we neglect the sensitivity of the partial derivatives to the state at which they are calculated.

Values of δR_{vi} , ε , h , δT_s , and z , are diagnosed using LMDZ-iso simulations. As an example $R_p(\delta R_{vi2}, \varepsilon_2, h_2, \delta T_{s2}, z_2)$ is the precipitation composition simulated by LMDZ for climate state 2. As another example, $R_p(0,0,1, \delta T_{s1}, z_1)$ is the precipitation composition predicted by Eqs. (2)-(5) with $\delta R_{vi} = 0$ and using the near-surface air temperature as T_s simulated by LMDZ for climatic state 1 (see Table 1).

12

13 3 Results

14 3.1 Impact of TP uplift on Asian climate

Theoretically, the Tibetan Plateau has both mechanical and thermal effects on atmospheric dynamics that induce increase monsoon activity to the south and drive arid climate to the north (Broccoli and Manabe, 1992; Sato and Kimura, 2005). Thus modifying TP height is expected to alter these large-scale atmospheric dynamics and associated climate variables (namely temperature, precipitation, relative humidity (hereafter RH), cloud cover), and in turn to affect the isotopic signature of rainfall.

In LOW experiment, strong summer heating leads to the onset of a “Thermal Low” (TL) at the latitude of maximal insolation (ca. 32°N), similar to the present-day TL existing over the Sahara desert (Fig. S2). This structure is superimposed by large-scale subsidence linked to the descending branch of the Hadley cell, and both factors act to drive widespread aridity over TP area between ca 30°N and 40°N, associated with very low (<40%) RH values (Fig. S2). Subsidence also prevents the development of South Asian monsoon over the north Indian plane and favours aridity over this region. In winter, large-scale subsidence induces high surface pressures and creates a anticyclonic cell that prevents convection and humidity advection, resulting in low RH and annual rainfall amount ranging from 50 to 500 mm over TP area (Fig. 3).



1 Uplifting TP from 250m above sea-level (ASL) to half of its present-day altitude (INT case)
2 initiates convection in the first tropospheric layers, restraining large-scale subsidence to the
3 upper levels (Fig. 3). In turn, south Asian monsoon is strengthened and associated northward
4 moisture transport and precipitation increase south of TP (Fig. 4, 5). As a consequence the
5 hydrological cycle over TP is more active, with higher evaporation rates (Fig. 6 D). Together
6 with colder temperatures linked to higher altitude (adiabatic effect) (Fig. 6 B), the stronger
7 hydrological cycle drives an increase in RH (Fig. 6 A) and cloud cover (Fig. S3). Another
8 consequence of increased altitude is higher snowfall rates in winter and associated rise of
9 surface albedo (fig. S4). When added to the increased cloud cover effect, this last process
10 contributes to an extra cooling of air masses over the Plateau. To the north of TP, the initial
11 stage of uplift results in increased aridity (i.e. lower RH and rainfall) over the Tarim Basin
12 region. This pattern can be explained both by a barrier effect of southern topography and by
13 stationary waves strengthening, that results in subsidence to the north of TP. This latter
14 mechanism is consistent with pioneer studies which showed that mountain-related activation
15 of stationary waves prevented cyclonic activity over Central Asia and induced aridity over
16 this region (Broccoli and Manabe, 1992).

17 The impact of the terminal stage of TP uplift also drives an increase in RH over the Plateau,
18 especially during summer time, when a very active continental recycling (Fig. S5) makes RH
19 rise from 40% (INT) to 70% (MOD). Precipitation amount also increases significantly (Fig.
20 5), driven both by increased evaporation and water recycling during summer, and intense
21 snowfall during winter. The latter contributes to increase the surface albedo and associated
22 surface cooling during winter. Conversely, the uplift to a modern-like Plateau reduces RH
23 (down to 30%) north of the Plateau, and allows the onset of large arid areas. We infer that this
24 aridification is linked to a mechanical blocking of moisture transport, both by Tian Shan
25 topography for the winter westerlies, and the eastern flanks of TP for summer fluxes, since
26 despite changes in stationary waves structure and sensible heat (not shown), no marked shift
27 in subsidence between INT and MOD experiments is simulated. This result is consistent with
28 recent studies (Miao et al., 2012; Sun et al., 2009) that have suggested the potential
29 contribution of Pamir and Tian Shan rainshadow effect to aridification in Quad Basin and
30 creation of Taklamakan Desert.

31



1 **3.2 Response of precipitation $\delta^{18}\text{O}$ to TP uplift**

2 **3.2.1 Model validation**

3 The modern mean annual isotopic distribution is characterised by very depleted values of
4 $\delta^{18}\text{O}$ over the Himalayas and the southern Tibet (down to -18‰) and a shift to more positive
5 values (ranges from -11 to -13‰) over northern TP and Kunlun from 30°N to 35°N .
6 Precipitation $\delta^{18}\text{O}$ over Tarim Basin experiences an abrupt decrease compared to northern TP,
7 with values down to -16‰ . (Fig. 7 A). Overall, simulated annual mean $\delta^{18}\text{O}_p$ are consistent
8 with sparse observations from the International Atomic Energy Agency (IAEA) Global
9 Network of Isotopes in Precipitation and $\delta^{18}\text{O}$ in precipitation measurements compiled from
10 Caves et al. (2015) (Fig. 7 A). In general, model shows a good agreement with precipitation
11 and VSMOW-weighted modern surface waters $\delta^{18}\text{O}$, including stream, lake and spring waters
12 (data from Bershaw et al., 2012; Hren et al., 2009; Quade et al., 2011). This comparison
13 shows ability of our model to reproduce decrease in $\delta^{18}\text{O}$ from India subcontinent to
14 Himalayas foothills and with minimum values over the Himalayas. Simulated increase in $\delta^{18}\text{O}$
15 over the TP with the distance from the Himalayas is consistent with data sampled along a
16 southwest-northeast transect across the Plateau (Bershaw et al., 2012). Model-data
17 discrepancies occur over central Tibetan Plateau where measured data have extremely
18 positive values probably linked with surface processes including high recycling rate and
19 contamination of streams with groundwater, that shifts surface water $\delta^{18}\text{O}$ to more positive
20 values compared to those in precipitation (Bershaw et al., 2012).

21

22 **3.2.2 Simulated isotopic changes and signal decomposition**

23 To first order, increasing topography over TP leads to more negative $\delta^{18}\text{O}$ over the region
24 (Fig. 7). In the absence of topography, precipitation $\delta^{18}\text{O}$ follows a zonal pattern and
25 undergoes a weak latitudinal depletion on the way to the continental interior, except from
26 slight deviations over the Indian plane, central China and the Eastern part of the TP (Fig. 7 C).
27 At 40°N , i.e. the northern edge of modern TP, $\delta^{18}\text{O}$ values reaches -9‰ in LOW case,
28 compared to -14‰ in MOD case. For the INT case the latitudinal depletion from south to
29 north is stronger (ca. 0.4‰ per latitudinal degree), with $\delta^{18}\text{O}$ values ranging from -6‰ for the
30 lowered Himalayas foothills to -11‰ for northern and eastern margins of TP (Fig. 7 B).



1 The total difference in isotopic composition of precipitation, ΔR_p , between experiments (INT-
2 LOW, MOD-INT) is significant beyond the areas where the topography was reduced by the
3 experimental design (Fig. 8 A, Fig. 9 A). Substantial differences in $\delta^{18}\text{O}$ between MOD and
4 INT experiments are simulated over the southern TP (up to 10‰) and over the Tarim Basin
5 (up to 7‰). Between INT and LOW cases, the differences are over the margins of the TP,
6 over Pamir, Tian Shan and Nan Chan. We should note that the isotopic difference becomes
7 more important for the later stage of the plateau uplift. For clarity, we define two boxes, over
8 the northern (from 34°N to 38°N and from 88°E to 100°E) and southern (from 27°N to 33°N
9 and from 75°E to 95°E) part of TP.

10

11 **Direct topography effect on $\delta^{18}\text{O}$**

12 The direct effect of topography change is determined as the decomposition term $\frac{\partial R_p}{\partial z} \cdot \Delta z$ in
13 Eq. (8). For the initial stage of the uplift, the altitude effect produces a decrease in
14 precipitation $\delta^{18}\text{O}$ ranging from -1 to -3‰ (Fig. 8 B). For the terminal stage of the uplift, the
15 isotopic decrease linked with altitude goes up to -7‰ (Fig. 9 B). Differences between both
16 stages are linked to the non-linear relationship between $\delta^{18}\text{O}$ and elevation. Also for both
17 stages, the difference between ΔR_p and $\frac{\partial R_p}{\partial z} \cdot \Delta z$ is non-zero (Fig. 10 A, Fig. 11 A). These
18 differences are particularly marked for the terminal stage, for which $\frac{\partial R_p}{\partial z} \cdot \Delta z$ averages -5.5‰
19 over the northern part of TP (Fig. 11 A B), whereas the total isotopic change averages -3‰.
20 Locally, the difference between $\frac{\partial R_p}{\partial z} \cdot \Delta z$ and ΔR_p can reach +4‰. When averaged over the
21 southern box, $\frac{\partial R_p}{\partial z} \cdot \Delta z$ is less negative (-4‰) than ΔR_p (-4.6‰), with localized maximum
22 differences reaching -4‰. Offsets between $\frac{\partial R_p}{\partial z} \cdot \Delta z$ and ΔR_p are also detected for the initial
23 stage of the uplift (Fig. 10 A B), but are lower: they reach +2‰ over central TP but barely
24 reach 1‰ when averaged over southern and northern boxes. These offsets are related to
25 additional effects of uplift on $\delta^{18}\text{O}$ that are discussed in the following sections.

26

27 **Non-adiabatic temperature changes impact**

28 Besides the adiabatic temperature effects linked with the TP uplift, non-adiabatic temperature
29 changes can be identified, in relation with surface albedo and cloud cover changes depicted in



1 3.2.1. The term $\frac{\partial R_p}{\partial \delta T_s} \cdot \Delta \delta T_s$ in Eq. (8) (Table 1, line 3) is associated with these non-adiabatic
 2 effects, i.e. spatial variations of the temperature lapse rate. Figure 8 C and Figure 9 C show
 3 the portion of the total isotopic signal that is linked to this effect. It plays a modest role for the
 4 early phase of uplift (+1-2‰ locally), but is more important for the second stage. It
 5 contributes to 2-3‰ of total isotopic difference, with a positive sign over southeast TP
 6 interior, TP northern margins and Asia interior. Negative anomalies have the same magnitude,
 7 but are less widespread, localized over the TP interior (Fig. 19 C). Positive isotopic anomalies
 8 are associated with steeper lapse rate than expected based on adiabatic processes. Conversely,
 9 negative $\delta^{18}\text{O}$ anomalies that are observed over northern TP and over Pamir are explained by
 10 a weaker lapse rate than adiabatic. Overall, these variations represent between 7 and 15% (2-
 11 8% for the initial stage) of the processes that are not linked to topography (Fig. 10 D, E and
 12 11 D, E).

13

14 **Impact of RH changes during condensation process**

15 The term $\frac{\partial R_p}{\partial h} \cdot \Delta h$ in Eq. (8) depicts the portion of total isotopic signal ΔR_p linked to local RH
 16 change during condensation process (Table. 1, line 4). Over TP, $\frac{\partial R_p}{\partial h} \cdot \Delta h$ is positive for both
 17 uplift phases, and RH changes act as a counterbalance to the topography effect. $\frac{\partial R_p}{\partial h} \cdot \Delta h$
 18 reaches +6‰ for the late stage (Fig. 9 D), and maxima are located over western part and
 19 northern part of TP for both stages of the uplift. Equation (5) shows that this positive anomaly
 20 is directly related to the increase in RH described in 3.2.1. For the initial stage, $\frac{\partial R_p}{\partial h} \cdot \Delta h$
 21 depicts also positive values (up to +4‰) to the southwest of TP. When averaged over
 22 northern and southern boxes, the counterbalancing effect of RH on ΔR_p ranges from 1.5 to
 23 +3‰, and this effect represents up to 76% of all non-topographic processes (Fig. 10, 11).
 24 Interestingly, an opposite signal is simulated over the Tarim basin, where topography was
 25 kept constant in the three experiments. This signal is consistent with the previously-depicted
 26 decrease in RH over this region, in relation with rain-shadow effects and large-scale
 27 subsidence.

28

29 **Post-condensation processes impact**



1 Estimation of term $\frac{\partial R_p}{\partial \varepsilon} \cdot \Delta \varepsilon$, i.e. the change in isotopic difference between vapour and
 2 precipitation, allows to quantify the contribution of post-condensational processes to total
 3 ΔR_p signal (Fig. 8 E, 9 E). For both stages of uplift, $\frac{\partial R_p}{\partial \varepsilon} \cdot \Delta \varepsilon$ is mostly negative, indicating a
 4 depletion of R_p relatively to R_v with the uplift. Over the Plateau, contribution of post-
 5 condensational effects for the initial stage of uplift ranges from 25% to 46% of total non-
 6 topographic effects, whereas it represents less than 10% for the terminal stage (Fig. 10 A, 11
 7 A). The most significant signal is simulated over the northern part of the Plateau and over its
 8 western margin and adjacent areas. Post-condensational effects during the initial stage lead to
 9 up to a -5‰ anomaly over the western margin of TP (Fig. 10 E) whereas the terminal stage
 10 creates a substantial negative anomaly only over northern TP margin and Tarim Basin
 11 (Fig. 11 E).

12

13 Residual processes effect

14 The last term of Eq. (8), $\frac{\partial R_p}{\partial R_{vi}} \cdot \Delta \delta R_{vi}$, corresponds to the part of the total isotopic signal that
 15 could not be explained by previously mentioned processes. These residual anomalies are
 16 rather weak for the initial stage of the uplift, explaining less than 1‰ of the signal over the
 17 northern plateau, and around 1‰ over the southern TP and adjacent parts of Asia and India
 18 (Fig. 8 F). Contribution of these effects to the initial stage is 4% and 21% to the northern and
 19 southern box respectively (Fig. 10 D E). Conversely, for the terminal stage of the TP uplift
 20 this anomaly reaches up to -4‰ over the southern part of the TP (Fig. 9 F) and contributes to
 21 49% of the non-topographic processes signal (Fig. 11 D E). In the next sections we propose
 22 several mechanisms that could contribute to this residual anomaly.

23

24 4 Discussion

25 Our results suggest that TP uplift affects precipitation $\delta^{18}\text{O}$ through direct topographic effect,
 26 but that a significant part of the signal is related to several other processes. These processes
 27 alter the isotopic signal not only over TP, but also over adjacent regions, where topography
 28 was kept the same by the experiment design. A second result is that despite a similar
 29 altitudinal change of TP between the two uplift stages, the topographic effect on $\delta^{18}\text{O}$ is more
 30 perturbed by other processes during the terminal stage than during the initial one.



1 For the terminal stage, the residual effects change over the southern region dominates (49%)
2 the isotopic signal that is not linked to the direct topographic effect. The RH change and non-
3 adiabatic temperature changes also have an important counterbalancing impact, together
4 contributing to 43% of the isotopic signal (Fig. 11 E). For the northern region, the topographic
5 effect is mainly counterbalanced by the RH change effect (2.5‰), ultimately leading to a
6 2.3‰ offset between ΔR_p and what expected from topography. Here RH contributes to 76%
7 of the isotopic signal not linked with the topography change, while non-adiabatic temperature
8 changes, residual effects change and post-condensational processes have an impact of 16%,
9 7% and <1% respectively (Fig. 11 D).

10

11 **4.1 Impact of RH variations**

12 RH alters rainfall isotopic signature through two steps, during and after condensation. As
13 mentioned earlier, the first effect of RH, as shown in Eq. (5) and expressed as $\frac{\partial R_p}{\partial h} \cdot \Delta h$, occurs
14 during condensation through Rayleigh distillation and induces that R_p increases with
15 increasing RH. Our model shows that RH increases over TP with the initial stage of uplift,
16 driving precipitation $\delta^{18}\text{O}$ towards less negative values. This mechanism is more efficient for
17 the terminal stage of uplift, when RH is increased in summer as a response of a more active
18 water cycle. South of TP, RH direct effect on $\delta^{18}\text{O}$ is noticeable, as efficient moisture
19 transport is activated with the uplift-driven strengthening of monsoon circulation (Fig. 4).
20 Interestingly, this mechanism is not active for the second stage of the uplift, during which
21 rainfall increases through more effective convection, not through higher advection of
22 moisture. As a consequence, negligible RH and R_p changes are simulated south of the Plateau
23 when it reaches its full height. This suggests that an altitudinal threshold might trigger south
24 Asian monsoon strengthening, and ultimately precipitation $\delta^{18}\text{O}$ signature, a hypothesis that
25 should be explored in further studies. Conversely, the negative values of $\frac{\partial R_p}{\partial h} \cdot \Delta h$ over and
26 northeast of the Tarim basin are related to a decrease in RH during both stages. Our analysis
27 suggests that the first uplift stage is sufficient to create both barrier effects to moisture fluxes
28 and large-scale subsidence that ultimately drive aridity over the region.

29 The second effect of RH on $\delta^{18}\text{O}$ concerns very dry areas (ca. < 40%), where raindrop re-
30 evaporation can occur after initial condensation, leading to an isotopic enrichment of
31 precipitation compared to water vapour (Lee and Fung, 2008) (Fig. S2). Such an effect is



1 implicitly included in the post-condensational term of our decomposition that shows opposite
2 sign when compared to $\frac{\partial R_p}{\partial h} \cdot \Delta h$. Over the Plateau, this mechanism is effective only for the
3 first uplift stage, where TP area transits from very low precipitation amounts and very low RH
4 values to wetter conditions (Fig. S6).

5 Over TP, the opposed effects of RH almost compensate each other for the early stage of the
6 uplift (Fig. 8 D, E), but it is not the case for the final stage, since RH post-condensational
7 effect is similar between INT and MOD experiments. Since absolute values of the impact of
8 RH through condensation and post-condensational processes can reach 5‰, it is crucial to
9 consider RH variation when inferring paleoaltitudes from carbonates $\delta^{18}\text{O}$.

10

11 **4.2 “Amount effect” and monsoon intensification**

12 Our results also show a substantial increase in precipitation amount over northern India, the
13 Himalayas and TP with the growth of topography for both uplift stages (Fig. 12). The inverse
14 relation between the enrichment in heavy isotopes in precipitation and precipitation amount,
15 named the “amount effect” (Dansgaard, 1964) is largely known for oceanic tropical
16 conditions (Risi et al., 2008; Rozanski, Kazimierz Araguás-Araguás and Gonfiantini, 1993)
17 and for Asia monsoonal areas (Lee et al., 2012; Yang et al., 2011). Over South Tibet recent
18 studies have shown the role of deep convection in isotopic depletion (He et al., 2015). For the
19 two stages of uplift, the residual component of the isotopic signal depicts negative values over
20 southern TP, where annual rainfall amount is increased. Thus we infer that this anomaly can
21 be driven, at least partly, by the amount effect that increases with growing topography.

22 Various climate studies have suggested that the appearance of the monsoonal system in East
23 Asia and the onset of central Asian desertification were related to Cenozoic Himalayan–
24 Tibetan uplift and withdrawal of the Paratethys Sea (Clift et al., 2008; Guo et al., 2002, 2008;
25 Kutzbach et al., 1989, 1993; Ramstein et al., 1997; Raymo and Ruddiman, 1992; Ruddiman
26 and Kutzbach, 1989; Sun and Wang, 2005; Zhang et al., 2007; Zhisheng et al., 2001) although
27 the exact timing of the monsoon onset and its intensification remains debated (Licht et al.,
28 2014; Molnar et al., 2010). Although our experimental setup, which does not include
29 Cenozoic paleogeography, was not designed to assess the question of monsoon driving
30 mechanisms nor its timing, our results suggest that uplifting the Plateau from 250 meters ASL
31 to half of its present height is enough to enhance moisture transport towards northern India



1 and strengthen seasonal rainfall. Nevertheless, massive increase of rainfall over TP between
2 INT and MOD experiments indicates that the second phase of uplift might be crucial to
3 activate an efficient, modern-day-like, hydrological cycle over the Plateau. The decrease in
4 simulated precipitation north of the Plateau also suggests that terminal phase of TP uplift
5 triggered modern-day arid areas.

6

7 **4.3 Other effects**

8 Although precipitation amount change explains well the residual isotopic anomaly (Fig. 8 F,
9 Fig. 9 F), additional processes could interplay. Continental recycling can overprint original
10 moisture signature and shifts the isotopic ratios to higher values due to recharging of moisture
11 by heavy isotopes from soil evaporation (Lee et al., 2012; Risi et al., 2013). In our simulation,
12 we detect an increasing role of continental recycling in the hydrological budget of the TP
13 (Fig. S5), especially in its central part, that likely shifts the $\delta^{18}\text{O}$ to more positive values and
14 partially compensate for the depletion linked to the “amount effect” over the central plateau.
15 Another process frequently invoked to explain the evolution of precipitation $\delta^{18}\text{O}$ patterns
16 over TP is changes in moisture sources (Bershaw et al., 2012; Dettman et al., 2003; Quade et
17 al., 2007; Tian et al., 2007). Except for the continentally recycled moisture, southern
18 Himalayas precipitation moisture originates mainly from the Indian, the Atlantic and the
19 Pacific Oceans (Fig. S5). Proximate oceanic basins are known to be sources of moisture with
20 more positive signature than remote ones (Chen et al., 2012; Gat, 1996). Supplemental
21 analyses with water-tagging feature of LMDZiso show that contribution of continental
22 recycling to rainfall over TP increases with the uplift, at the expense of Pacific and Indian
23 sources (Fig. S5). Although we have no mean to decipher between sources and amount effect
24 in the residual anomaly, it seems that the change of sources is not sufficient to yield a strong
25 offset of $\delta^{18}\text{O}$ values.

26

27 **4.4 Relevance of paleoelevation reconstructions based on paleo $\delta^{18}\text{O}$**

28 Quantitative paleoelevation reconstructions using modern altitude- $\delta^{18}\text{O}$ relationship will
29 succeed only if ΔR_p corresponds mainly to the direct topography effect. Modern
30 paleoaltimetry studies cover almost all regions of the Plateau for time periods ranging from
31 Palaeocene to Pleistocene-Quaternary (see data compilation in Caves et al., 2015). Most of



1 these studies consider changes in $\delta^{18}\text{O}$ as a direct effect of the topography uplift.
2 Paleoelevation studies locations (see Caves et al., 2015 for a synthesis) plotted over the
3 anomaly maps (Fig. 10 A, Fig. 11 A) show for what geographical regions restored elevations
4 should be used with an additional caution. Numerous paleoelevation data points were located
5 either over the northern part of the TP (from 34°N to 38°N and from 88°E to 100°E) or over
6 the southern region (from 27°N to 33°N and from 75°E to 95°E).

7 Our model results show that when TP altitude is increased from half to full, considering
8 topography as an exclusive controlling factor of precipitation $\delta^{18}\text{O}$ over the southern
9 (northern) region likely yield overestimations (underestimations) of surface uplift, since the
10 topography effect is offset by RH and amount effects. Projecting our modelling results to each
11 locality where paleoelevation studies have been published (Table 3) reveals that topography
12 change explains simulated total isotopic change reasonably well for only few locations
13 (Linzhou Basin, Lunpola Basin, Kailas Basin, Huaitoutala). Indeed topography appears to be
14 the main controlling factor for only 40% of the sites, while 30% are dominated by RH effects,
15 13% by residual effects and 5% and 2% by post-condensational and non-adiabatic
16 temperature changes, respectively. Nevertheless such figures have to be taken carefully, since
17 we ran idealized experiments testing only the impact of uplift, neglecting other factors like
18 horizontal paleogeography or pCO_2 variations, the latter being known to influence $\delta^{18}\text{O}$ as
19 well (Jeffery et al., 2012; Poulsen and Jeffery, 2011).

20 For the initial uplift stage apparent consistency occurs between the topography impact and the
21 total isotopic composition is observed, in relation with counteracting effects RH and pots-
22 condensational processes. For the southern region RH impact is appeared to be the main
23 controlling factor for the isotopic composition of precipitation, surpassing the direct
24 topography impact. Nevertheless, these processes have a different contribution for initial and
25 terminal stages of uplift. Precipitation changes lead to overestimate altitude changes for both
26 stages, but for the terminal stage its contribution is bigger. This effect dominates in the
27 southern part, and more generally where the isotopic composition of precipitation strongly
28 depends on convective activity. RH changes dominate over the western part of TP and
29 Northern India for initial uplift stage and over the northern TP for the terminal.

30



1 5 Conclusions

2 Previous studies focusing on the Andes (Ehlers and Poulsen, 2009; Poulsen et al., 2010) or
3 north American cordillera (Sewall and Fricke, 2013) have inferred that the impact of uplift of
4 mountain ranges on $\delta^{18}\text{O}$ could be altered by the consequences of the uplift on atmospheric
5 physics and dynamics. Our modelling results show that it is also the case for the Tibetan
6 Plateau uplift. Additionally, we designed a decomposing analysis to quantify for the first time
7 the different processes that can alter precipitation $\delta^{18}\text{O}$ changes with uplift. As suggested for
8 the Andes, the onset of convective rainfall plays an important role in shifting $\delta^{18}\text{O}$ towards
9 more negative values. Nevertheless this process is not the main factor, as we show that
10 saturation of air masses, quantified by RH have two to three-time bigger effects on the final
11 $\delta^{18}\text{O}$. We infer that increase in precipitation linked with the TP uplift would lead to
12 overestimation of the topography uplift at sites over Himalayas and Southern TP, whereas
13 increase in RH leads to underestimating the uplift at sites in Northern Tibet.

14 Our results could be applied to interpret paleoclimate records and to reconstruct the region
15 uplift history. Paleoelevation reconstructions suggest the Himalayas attained their current
16 elevation by the late Miocene (Garzzone et al., 2000a, 2000b; Rowley et al., 2001; Saylor et
17 al., 2009). Our results show overestimation of the topography impact over this region, thus the
18 Himalayas may have attained their current elevation later than expected. In contrast, isotope-
19 based paleoaltimetry could underestimate surface elevation over the northern TP. This could
20 explain why available isotope-based paleoelevation estimates for the northern TP (Cyr et al.,
21 2005), which estimates surface elevation about 2km, contradict palynological assemblages in
22 lacustrine sediments from the Xining basin, which show the presence of high-altitude
23 vegetation at the same time period (Dupont-Nivet et al., 2008; Hoorn et al., 2012).

24 Still, our decomposition methods reveal that even if the impact of the TP uplift phases are
25 rather straightforward (monsoon enhancement to the South, increase in continental recycling
26 over TP, moisture fluxes deflection and increased aridity to the North), the consequences in
27 terms of $\delta^{18}\text{O}$ are extremely complex, since interplays and compensation occur amongst all
28 the processes. Limitations in our approach are related to 1/ the theoretical uplift scenario we
29 chose, and 2/ the fact that all other boundary conditions are set to present. Concerning the
30 latter, changes in vegetation cover, by altering albedo and persistence of snow cover, could
31 affect the impact of non-adiabatic temperature changes on $\delta^{18}\text{O}$. Vegetation over Asia was
32 shown to have a major variation through Cenozoic based on pollen (Dupont-Nivet et al.,



1 2008; Miao et al., 2011; Song et al., 2010; Zhao and Yu, 2012) and paleobotanical data (An
2 et al., 2005; De Franceschi et al., 2008; Kohn, 2010) and future studies would benefit to
3 explore its impact on precipitation $\delta^{18}\text{O}$. Also it is largely known that during the Cenozoic air
4 temperature was higher due to higher concentration of greenhouse gases in the atmosphere
5 (Zachos et al., 2008). Studies taking into account this feedback inferred that it could lead to
6 even larger inaccuracy in surface uplift estimations during the Cenozoic (Poulsen and Jeffery,
7 2011). Thus the field of paleoaltimetry would benefit from future studies applying a
8 decomposition method and comparing paleoaltitude data to GCM simulations forced by
9 constrained paleogeography (land-sea mask and different scenarios for orogens) and
10 atmospheric pCO_2 .

11

12 **Acknowledgements**

13 This work is a part of iTECC (interaction Tectonics-Erosion-Climate-Coupling) project
14 funded by European Union. Computational resources were provided by IDRIS-GENCI
15 (project 0292), France

16

17 **References**

18 An, Z., Huang, Y., Liu, W., Guo, Z., Clemens, S., Li, L., Prell, W., Ning, Y., Cai, Y., Zhou,
19 W., Lin, B., Zhang, Q., Cao, Y., Qiang, X., Chang, H. and Wu, Z.: Multiple expansions of C4
20 plant biomass in East Asia since 7 Ma coupled with strengthened monsoon circulation,
21 *Geology*, 33(9), 705–708, doi:10.1130/G21423.1, 2005.

22 Bershaw, J., Penny, S. M. and Garziona, C. N.: Stable isotopes of modern water across the
23 Himalaya and eastern Tibetan Plateau: Implications for estimates of paleoelevation and
24 paleoclimate, *J. Geophys. Res. Atmos.*, 117(2), 1–18, doi:10.1029/2011JD016132, 2012.

25 Boos, W. R. (yale): A review of recent progress on Tibet's role in the South Asian monsoon,
26 *Clivar*, (1996), 2015.

27 Broccoli, A. J. and Manabe, S.: The Effects of Orography on Midlatitude Northern
28 Hemisphere Dry Climates, *J. Clim.*, 5(11), 1181–1201, doi:10.1175/1520-
29 0442(1992)005<1181:teoom>2.0.co;2, 1992.

30 Caves, J. K., Winnick, M. J., Graham, S. A., Sjostrom, D. J., Mulch, A. and Chamberlain, C.



- 1 P.: Role of the westerlies in Central Asia climate over the Cenozoic, *Earth Planet. Sci. Lett.*,
2 428, 33–43, 2015.
- 3 Chen, B., Xu, X. De, Yang, S. and Zhang, W.: On the origin and destination of atmospheric
4 moisture and air mass over the Tibetan Plateau, *Theor. Appl. Climatol.*, 110(3), 423–435,
5 doi:10.1007/s00704-012-0641-y, 2012.
- 6 Chen, G.-S., Liu, Z. and Kutzbach, J. E.: Reexamining the barrier effect of the Tibetan
7 Plateau on the South Asian summer monsoon, *Clim. Past*, 10(3), 1269–1275, doi:10.5194/cp-
8 10-1269-2014, 2014.
- 9 Clift, P. D., Hodges, K. V., Heslop, D., Hannigan, R., Van Long, H. and Calves, G.:
10 Correlation of Himalayan exhumation rates and Asian monsoon intensity, *Nat. Geosci.*, 1(12),
11 875–880, doi:10.1038/ngeo351, 2008.
- 12 Currie, B. S., Rowley, D. B. and Tabor, N. J.: Middle Miocene paleoaltimetry of southern
13 Tibet: Implications for the role of mantle thickening and delamination in the Himalayan
14 orogen, *Geology*, 33(3), 181–184, doi:10.1130/G21170.1, 2005.
- 15 Cyr, A. J., Currie, B. S. and Rowley, D. B.: Geochemical Evaluation of Fenghuoshan Group
16 Lacustrine Carbonates, North-Central Tibet: Implications for the Palealtimetry of the Eocene
17 Tibetan Plateau, *J. Geol.*, 113(5), 517–533, doi:10.1086/431907, 2005.
- 18 Dansgaard, W.: Stable isotopes in precipitation, *Tellus A*, doi:10.3402/tellusa.v16i4.8993,
19 1964.
- 20 DeCelles, P. G., Quade, J., Kapp, P., Fan, M., Dettman, D. L. and Ding, L.: High and dry in
21 central Tibet during the Late Oligocene, *Earth Planet. Sci. Lett.*, 253(3-4), 389–401,
22 doi:10.1016/j.epsl.2006.11.001, 2007.
- 23 Dettman, D. L., Fang, X., Garzzone, C. N. and Li, J.: Uplift-driven climate change at 12 Ma:
24 A long $\delta^{18}\text{O}$ record from the NE margin of the Tibetan plateau, *Earth Planet. Sci. Lett.*, 214(1-
25 2), 267–277, doi:10.1016/S0012-821X(03)00383-2, 2003.
- 26 Ding, L., Xu, Q., Yue, Y., Wang, H., Cai, F. and Li, S.: The Andean-type Gangdese
27 Mountains: Paleoelevation record from the Paleocene-Eocene Linzhou Basin, *Earth Planet.*
28 *Sci. Lett.*, 392, 250–264, doi:10.1016/j.epsl.2014.01.045, 2014.
- 29 Dupont-Nivet, G., Hoom, C. and Konert, M.: Tibetan uplift prior to the Eocene-Oligocene
30 climate transition: Evidence from pollen analysis of the Xining Basin, *Geology*, 36(12), 987–



- 1 990, doi:10.1130/G25063A.1, 2008.
- 2 Ehlers, T. A. and Poulsen, C. J.: Influence of Andean uplift on climate and paleoaltimetry
3 estimates, *Earth Planet. Sci. Lett.*, 281(3-4), 238–248, doi:10.1016/j.epsl.2009.02.026, 2009.
- 4 Forest, C. E., Wolfe, J. A., Molnar, P. and Emanuel, K. A.: Paleoaltimetry incorporating
5 atmospheric physics and botanical estimates of paleoclimate, *Geol. Soc. Am. Bull.*, 111(4),
6 497–511, doi:10.1130/0016-7606(1999)111<0497:PIAPAB>2.3.CO;2, 1999.
- 7 De Franceschi, D., Hoorn, C., Antoine, P. O., Cheema, I. U., Flynn, L. J., Lindsay, E. H.,
8 Marivaux, L., Métais, G., Rajpar, A. R. and Welcomme, J. L.: Floral data from the mid-
9 Cenozoic of central Pakistan, *Rev. Palaeobot. Palynol.*, 150, 115–129,
10 doi:10.1016/j.revpalbo.2008.01.011, 2008.
- 11 Frankenberg, C., Yoshimura, K., Warneke, T., Aben, I., Butz, A., Deutscher, N., Griffith, D.,
12 Hase, F., Notholt, J., Schneider, M., Schrijver, H. and Röckmann, T.: Dynamic Processes
13 Governing Lower-Tropospheric HDO/H₂O Ratios as Observed from Space and Ground,
14 *Science (80-.)*, 325(5946), 1374–1377, doi:10.1126/science.1173791, 2009.
- 15 Galewsky, J. and Hurley, J. V.: An advection-condensation model for subtropical water vapor
16 isotopic ratios, *J. Geophys. Res. Atmos.*, 115(D16), 2010.
- 17 Galewsky, J., Sobel, A. and Held, I.: Diagnosis of subtropical humidity dynamics using
18 tracers of last saturation, *J. Atmos. Sci.*, 62(9), 3353–3367, 2005.
- 19 Garzzone, C. N., Dettman, D. L., Quade, J., De Celles, P. G. and Butler, R. F.: High times on
20 the Tibetan Plateau: Paleoelevation of the Thakkhola graben, Nepal, *Geology*, 28(4), 339–
21 342, doi:10.1130/0091-7613(2000)28<339:HTOTTP>2.0.CO;2, 2000a.
- 22 Garzzone, C. N., Quade, J., DeCelles, P. G. and English, N. B.: Predicting paleoelevation of
23 Tibet and the Himalaya from $\delta^{18}\text{O}$ vs. altitude gradients in meteoric water across the Nepal
24 Himalaya, *Earth Planet. Sci. Lett.*, 183(1-2), 215–229, doi:10.1016/S0012-821X(00)00252-1,
25 2000b.
- 26 Gat, J. R.: Oxygen and hydrogen isotopes in the hydrologic cycle, *Annu. Rev. Earth Planet.*
27 *Sci.*, 24(1), 225–262, 1996.
- 28 Gedzelman, S. D. and Arnold, R.: Modeling the isotopic composition of precipitation, New
29 York, 99, 1994.
- 30 Guo, Z. T., Ruddiman, W. F., Hao, Q. Z., Wu, H. B., Qiao, Y. S., Zhu, R. X., Peng, S. Z.,



- 1 Wei, J. J., Yuan, B. Y. and Liu, T. S.: Onset of Asian desertification by 22 Myr ago inferred
2 from loess deposits in China., *Nature*, 416(6877), 159–163, doi:10.1038/416159a, 2002.
- 3 Guo, Z. T., Sun, B., Zhang, Z. S., Peng, S. Z., Xiao, G. Q., Ge, J. Y., Hao, Q. Z., Qiao, Y. S.,
4 Liang, M. Y., Liu, J. F., Yin, Q. Z. and Wei, J. J.: A major reorganization of Asian climate by
5 the early Miocene, *Clim. Past*, 4(3), 153–174, doi:10.5194/cp-4-153-2008, 2008.
- 6 Harris, N.: The elevation history of the Tibetan Plateau and its implications for the Asian
7 monsoon, *Palaeogeogr. Palaeoclimatol. Palaeoecol.*, 241(1), 4–15,
8 doi:10.1016/j.palaeo.2006.07.009, 2006.
- 9 He, Y., Risi, C., Gao, J., Masson-delmotte, V., Yao, T., Lai, C., Ding, Y., Worden, J.,
10 Frankenberg, C., Chepfer, H. and Cesana, G.: Special Section : Impact of atmospheric
11 convection on south Tibet summer precipitation isotopologue composition using a
12 combination of in situ measurements, satellite data, and atmospheric general circulation
13 modeling, , 3852–3871, doi:10.1002/2014JD022180.Abstract, 2015.
- 14 Hoke, G. D., Liu-Zeng, J., Hren, M. T., Wissink, G. K. and Garziona, C. N.: Stable isotopes
15 reveal high southeast Tibetan Plateau margin since the Paleogene, *Earth Planet. Sci. Lett.*,
16 394, 270–278, doi:10.1016/j.epsl.2014.03.007, 2014.
- 17 Hoorn, C., Straathof, J., Abels, H. a., Xu, Y., Utescher, T. and Dupont-Nivet, G.: A late
18 Eocene palynological record of climate change and Tibetan Plateau uplift (Xining Basin,
19 China), *Palaeogeogr. Palaeoclimatol. Palaeoecol.*, 344-345, 16–38,
20 doi:10.1016/j.palaeo.2012.05.011, 2012.
- 21 Hourdin, F., Musat, I., Bony, S., Braconnot, P., Codron, F., Dufresne, J. L., Fairhead, L.,
22 Filiberti, M. A., Friedlingstein, P., Grandpeix, J. Y., Krinner, G., LeVan, P., Li, Z. X. and
23 Lott, F.: The LMDZ4 general circulation model: Climate performance and sensitivity to
24 parametrized physics with emphasis on tropical convection, *Clim. Dyn.*, 27(7-8), 787–813,
25 doi:10.1007/s00382-006-0158-0, 2006.
- 26 Hren, M. T., Bookhagen, B., Blisniuk, P. M., Booth, A. L. and Chamberlain, C. P.: $\delta^{18}\text{O}$ and
27 δD of streamwaters across the Himalaya and Tibetan Plateau: Implications for moisture
28 sources and paleoelevation reconstructions, *Earth Planet. Sci. Lett.*, 288(1-2), 20–32,
29 doi:10.1016/j.epsl.2009.08.041, 2009.
- 30 Jeffery, M. L., Poulsen, C. J. and Ehlers, T. A.: Impacts of Cenozoic global cooling, surface
31 uplift, and an inland seaway on South American paleoclimate and precipitation $\delta^{18}\text{O}$, *Geol.*



- 1 Soc. Am. Bull., 124(3-4), 335–351, 2012.
- 2 Kattel, D. B., Yao, T., Yang, W., Gao, Y. and Tian, L.: Comparison of temperature lapse rates
3 from the northern to the southern slopes of the Himalayas, *Int. J. Climatol.*, 2015.
- 4 Khan, M. A., Spicer, R. a., Bera, S., Ghosh, R., Yang, J., Spicer, T. E. V, Guo, S. X., Su, T.,
5 Jacques, F. and Grote, P. J.: Miocene to Pleistocene floras and climate of the Eastern
6 Himalayan Siwaliks, and new palaeoelevation estimates for the Namling-Oiyug Basin, Tibet,
7 *Glob. Planet. Change*, 113, 1–10, doi:10.1016/j.gloplacha.2013.12.003, 2014.
- 8 Kohn, M. J.: Carbon isotope compositions of terrestrial C₃ plants as indicators of
9 (paleo)ecology and (paleo)climate, *Proc. Natl. Acad. Sci.*, 107(46), 19691–19695,
10 doi:10.1073/pnas.1004933107, 2010.
- 11 Kutzbach, J. E., Guetter, P. J., Ruddiman, W. F. and Prell, W. L.: Sensitivity of climate to late
12 Cenozoic uplift in southern Asia and the American west: numerical experiments, *J. Geophys.*
13 *Res. Atmos.*, 94(D15), 18393–18407, 1989.
- 14 Kutzbach, J. E., Prell, W. L. and Ruddiman, W. F.: Sensitivity of Eurasian climate to surface
15 uplift of the Tibetan Plateau, *J. Geol.*, 177–190, 1993.
- 16 Ladant, J., Donnadieu, Y., Lefebvre, V. and Dumas, C.: The respective role of atmospheric
17 carbon dioxide and orbital parameters on ice sheet evolution at the Eocene-Oligocene
18 transition, *Paleoceanography*, 29(8), 810–823, doi:10.1002/2013PA002593, 2014.
- 19 Lee, J. and Fung, I.: “Amount effect” of water isotopes and quantitative analysis of post-
20 condensation processes, *Hydrol. Process.*, 22(1), 1–8, 2008.
- 21 Lee, J. E., Risi, C., Fung, I., Worden, J., Scheepmaker, R. A., Lintner, B. and Frankenberg,
22 C.: Asian monsoon hydrometeorology from TES and SCIAMACHY water vapor isotope
23 measurements and LMDZ simulations: Implications for speleothem climate record
24 interpretation, *J. Geophys. Res. Atmos.*, 117(15), 1–12, doi:10.1029/2011JD017133, 2012.
- 25 Van Leer, B.: Towards the ultimate conservative difference scheme. IV. A new approach to
26 numerical convection, *J. Comput. Phys.*, 23(3), 276–299, doi:http://dx.doi.org/10.1016/0021-
27 9991(77)90095-X, 1977.
- 28 LeGrande, A. N. and Schmidt, G. A.: Sources of Holocene variability of oxygen isotopes in
29 paleoclimate archives, *Clim. Past*, 5(3), 441–455, doi:10.5194/cp-5-441-2009, 2009.
- 30 Li, S., Currie, B. S., Rowley, D. B. and Ingalls, M.: Cenozoic paleoaltimetry of the SE margin



- 1 of the Tibetan Plateau: Constraints on the tectonic evolution of the region, *Earth Planet. Sci.*
2 *Lett.*, 432, 415–424, doi:10.1016/j.epsl.2015.09.044, 2015.
- 3 Licht, A., van Cappelle, M., Abels, H. A., Ladant, J.-B., Trabucho-Alexandre, J., France-
4 Lanord, C., Donnadiou, Y., Vandenberghe, J., Rigaudier, T., Lécuyer, C., Terry Jr, D.,
5 Adriaens, R., Boura, A., Guo, Z., Soe, A. N., Quade, J., Dupont-Nivet, G. and Jaeger, J.-J.:
6 Asian monsoons in a late Eocene greenhouse world, *Nature*, 513(7519), 501–506,
7 doi:10.1038/nature13704, 2014.
- 8 Liu, X., Sun, H., Miao, Y., Dong, B. and Yin, Z.-Y.: Impacts of uplift of northern Tibetan
9 Plateau and formation of Asian inland deserts on regional climate and environment, *Quat. Sci.*
10 *Rev.*, 116, 1–14, doi:10.1016/j.quascirev.2015.03.010, 2015.
- 11 McElwain, J. C.: Climate-independent paleoaltimetry using stomatal density in fossil leaves
12 as a proxy for CO₂ partial pressure, *Geology*, 32(12), 1017, doi:10.1130/G20915.1, 2004.
- 13 Merlivat, L. and Nief, G.: Fractionnement isotopique lors des changements d'état solide-
14 vapeur et liquide-vapeur de l'eau à des températures inférieures à 0°C, *Tellus*, 19(1), 122–127,
15 doi:10.1111/j.2153-3490.1967.tb01465.x, 1967.
- 16 Miao, Y., Fang, X., Herrmann, M., Wu, F., Zhang, Y. and Liu, D.: Miocene pollen record of
17 KC-1 core in the Qaidam Basin, NE Tibetan Plateau and implications for evolution of the
18 East Asian monsoon, *Palaeogeogr. Palaeoclimatol. Palaeoecol.*, 299(1-2), 30–38,
19 doi:10.1016/j.palaeo.2010.10.026, 2011.
- 20 Miao, Y., Herrmann, M., Wu, F., Yan, X. and Yang, S.: What controlled Mid-Late Miocene
21 long-term aridification in Central Asia? - Global cooling or Tibetan Plateau uplift: A review,
22 *Earth-Science Rev.*, 112(3-4), 155–172, doi:10.1016/j.earscirev.2012.02.003, 2012.
- 23 Molnar, P., Boos, W. R. and Battisti, D. S.: Orographic Controls on Climate and Paleoclimate
24 of Asia: Thermal and Mechanical Roles for the Tibetan Plateau, *Annu. Rev. Earth Planet.*
25 *Sci.*, 38(1), 77–102, doi:10.1146/annurev-earth-040809-152456, 2010.
- 26 Mulch, A.: Stable isotope paleoaltimetry and the evolution of landscapes and life, *Earth*
27 *Planet. Sci. Lett.*, 433, 180–191, doi:10.1016/j.epsl.2015.10.034, 2016.
- 28 Pausata, F. S. R., Battisti, D. S., Nisancioglu, K. H. and Bitz, C. M.: Chinese stalagmite $\delta^{18}\text{O}$
29 controlled by changes in the Indian monsoon during a simulated Heinrich event, *Nat. Geosci.*,
30 4(7), 474–480, doi:10.1038/ngeo1169, 2011.



- 1 Poage, M. A. and Chamberlain, C. P.: Empirical relationships between elevation and the
2 stable isotope composition of precipitation and surface waters: Considerations for studies of
3 paleoelevation change, *Am. J. Sci.*, 301(1), 1–15, doi:10.2475/ajs.301.1.1, 2001.
- 4 Pohl, A., Donnadieu, Y., Le Hir, G., Buoncristiani, J.-F. and Vennin, E.: Effect of the
5 Ordovician paleogeography on the (in)stability of the climate, *Clim. Past*, 10(6), 2053–2066,
6 doi:10.5194/cp-10-2053-2014, 2014.
- 7 Polissar, P. J., Freeman, K. H., Rowley, D. B., McInerney, F. a. and Currie, B. S.:
8 Palealtimetry of the Tibetan Plateau from D/H ratios of lipid biomarkers, *Earth Planet. Sci.*
9 *Lett.*, 287(1-2), 64–76, doi:10.1016/j.epsl.2009.07.037, 2009.
- 10 Poulsen, C. J. and Jeffery, M. L.: Climate change imprinting on stable isotopic compositions
11 of high-elevation meteoric water cloaks past surface elevations of major orogens, *Geology*,
12 39(6), 595–598, doi:10.1130/G32052.1, 2011.
- 13 Poulsen, C. J., Ehlers, T. a and Insel, N.: Onset of convective rainfall during gradual late
14 Miocene rise of the central Andes., *Science*, 328(5977), 490–493,
15 doi:10.1126/science.1185078, 2010.
- 16 Quade, J., Garziona, C. and Eiler, J.: Paleoelevation Reconstruction using Pedogenic
17 Carbonates, *Rev. Mineral. Geochemistry*, 66(1), 53–87, doi:10.2138/rmg.2007.66.3, 2007.
- 18 Quade, J., Brecker, D. O., Daëron, M. and Eiler, J.: The palealtimetry of Tibet: An isotopic
19 perspective, *Am. J. Sci.*, 311(2), 77–115, doi:10.2475/02.2011.01, 2011.
- 20 Ramstein, G., Fluteau, F., Besse, J. and Joussaume, S.: Effect of orogeny, plate motion and
21 land–sea distribution on Eurasian climate change over the past 30 million years, *Nature*,
22 386(6627), 788–795, doi:10.1038/386788a0, 1997.
- 23 Raymo, M. E. and Ruddiman, W. F.: Tectonic forcing of late Cenozoic climate, *Nature*,
24 359(6391), 117–122, 1992.
- 25 Risi, C., Bony, S. and Vimeux, F.: Influence of convective processes on the isotopic
26 composition ($\delta^{18}\text{O}$ and δD) of precipitation and water vapor in the tropics: 2. Physical
27 interpretation of the amount effect, *J. Geophys. Res. Atmos.*, 113(19), 1–12,
28 doi:10.1029/2008JD009943, 2008.
- 29 Risi, C., Bony, S., Vimeux, F. and Jouzel, J.: Water-stable isotopes in the LMDZ4 general
30 circulation model: Model evaluation for present-day and past climates and applications to



- 1 climatic interpretations of tropical isotopic records, *J. Geophys. Res. Atmos.*, 115(12), 1–27,
2 doi:10.1029/2009JD013255, 2010.
- 3 Risi, C., Noone, D., Frankenberg, C. and Worden, J.: Role of continental recycling in
4 intraseasonal variations of continental moisture as deduced from model simulations and water
5 vapor isotopic measurements, *Water Resour. Res.*, 49(7), 4136–4156,
6 doi:10.1002/wrcr.20312, 2013.
- 7 Rodwell, M. J. and Hoskins, B. J.: Subtropical anticyclones and summer monsoons, *J. Clim.*,
8 14(15), 3192–3211, 2001.
- 9 Rowley, D. B. and Currie, B. S.: Palaeo-altimetry of the late Eocene to Miocene Lunpola
10 basin, central Tibet., *Nature*, 439(7077), 677–681, doi:10.1038/nature04506, 2006.
- 11 Rowley, D. B. and Garzione, C. N.: Stable Isotope-Based Palealtimetry, *Annu. Rev. Earth
12 Planet. Sci.*, 35(1), 463–508, doi:10.1146/annurev.earth.35.031306.140155, 2007.
- 13 Rowley, D. B., Pierrehumbert, R. T. and Currie, B. S.: A new approach to stable isotope-
14 based palealtimetry: Implications for palealtimetry and paleohypsometry of the High
15 Himalaya since the late Miocene, *Earth Planet. Sci. Lett.*, 188(1-2), 253–268,
16 doi:10.1016/S0012-821X(01)00324-7, 2001.
- 17 Royden, L. H., Burchfiel, B. C. and Hilst, R. D. Van Der: The Geological Evolution of the
18 Tibetan Plateau, , 321(August), 1054–1058, 2008.
- 19 Rozanski, Kazimierz Araguás-Araguás, L. and Gonfiantini, R.: Isotopic patterns in modern
20 global precipitation, *Clim. Chang. Cont. Isot. Rec.*, 1–36, 1993.
- 21 Ruddiman, W. F. and Kutzbach, J. E.: Forcing of late Cenozoic northern hemisphere climate
22 by plateau uplift in southern Asia and the American West, *J. Geophys. Res. Atmos.*, 94(D15),
23 18409–18427, 1989.
- 24 Sato, T. and Kimura, F.: Impact of diabatic heating over the Tibetan Plateau on subsidence
25 over northeast Asian arid region, *Geophys. Res. Lett.*, 32(5), 1–5,
26 doi:10.1029/2004GL022089, 2005.
- 27 Saylor, J. E., Quade, J., Dettman, D. L., DeCelles, P. G., Kapp, P. A. and Ding, L.: The late
28 Miocene through present paleoelevation history of southwestern Tibet, *Am. J. Sci.*, 309(1), 1–
29 42, doi:10.2475/01.2009.01, 2009.
- 30 Sepulchre, P., Ramstein, G., Fluteau, F., Schuster, M., Tiercelin, J.-J. and Brunet, M.:



- 1 Tectonic uplift and Eastern Africa aridification., *Science*, 313(5792), 1419–1423,
2 doi:10.1126/science.1129158, 2006.
- 3 Sewall, J. O. and Fricke, H. C.: Andean-scale highlands in the Late Cretaceous Cordillera of
4 the North American western margin, *Earth Planet. Sci. Lett.*, 362, 88–98,
5 doi:10.1016/j.epsl.2012.12.002, 2013.
- 6 Sherwood, S. C.: Maintenance of the free-tropospheric tropical water vapor distribution. Part
7 II: Simulation by large-scale advection, *J. Clim.*, 9(11), 2919–2934, 1996.
- 8 Song, X. Y., Spicer, R. a., Yang, J., Yao, Y. F. and Li, C. Sen: Pollen evidence for an Eocene
9 to Miocene elevation of central southern Tibet predating the rise of the High Himalaya,
10 *Palaeogeogr. Palaeoclimatol. Palaeoecol.*, 297(1), 159–168,
11 doi:10.1016/j.palaeo.2010.07.025, 2010.
- 12 Stowhas, L. and Moyano, J. C.: Simulation of the Isotopic Content of Precipitation, *Atmos.*
13 *Environ. Part a-General Top.*, 27(3), 327–333, doi:10.1016/0960-1686(93)90106-9, 1993.
- 14 Sun, J., Zhang, Z. and Zhang, L.: New evidence on the age of the Taklimakan Desert,
15 *Geology*, 37(2), 159–162, doi:10.1130/G25338A.1, 2009.
- 16 Sun, J., Xu, Q., Liu, W., Zhang, Z., Xue, L. and Zhao, P.: Palynological evidence for the
17 latest Oligocene-early Miocene paleoelevation estimate in the Lunpola Basin, central Tibet,
18 *Palaeogeogr. Palaeoclimatol. Palaeoecol.*, 399, 21–30, doi:10.1016/j.palaeo.2014.02.004,
19 2014.
- 20 Sun, X. and Wang, P.: How old is the Asian monsoon system?—Palaeobotanical records from
21 China, *Palaeogeogr. Palaeoclimatol. Palaeoecol.*, 222(3–4), 181–222,
22 doi:http://dx.doi.org/10.1016/j.palaeo.2005.03.005, 2005.
- 23 Tapponnier, P., Zhiqin, X., Roger, F., Meyer, B., Arnaud, N., Wittlinger, G. and Jingsui, Y.:
24 Oblique stepwise rise and growth of the Tibet plateau., *Science*, 294(5547), 1671–1677,
25 doi:10.1126/science.105978, 2001.
- 26 Taylor, K. E., Williamson, D. and Zwiers, F.: The sea surface temperature and sea-ice
27 concentration boundary conditions for AMIP II simulations, Program for Climate Model
28 Diagnosis and Intercomparison, Lawrence Livermore National Laboratory, University of
29 California., 2000.
- 30 Tian, L., Yao, T., MacClune, K., White, J. W. C., Schilla, A., Vaughn, B., Vachon, R. and



- 1 Ichiyangi, K.: Stable isotopic variations in west China: A consideration of moisture sources,
2 J. Geophys. Res. Atmos., 112(10), 1–12, doi:10.1029/2006JD007718, 2007.
- 3 Vuille, M., Werner, M., Bradley, R. S., Chan, R. Y. and Keimig, F.: Stable isotopes in East
4 African precipitation record Indian Ocean zonal mode, Geophys. Res. Lett., 32(21), 1–5,
5 doi:10.1029/2005GL023876, 2005.
- 6 Xu, Q., Ding, L., Zhang, L., Cai, F., Lai, Q., Yang, D. and Liu-Zeng, J.: Paleogene high
7 elevations in the Qiangtang Terrane, central Tibetan Plateau, Earth Planet. Sci. Lett., 362, 31–
8 42, doi:10.1016/j.epsl.2012.11.058, 2013.
- 9 Yang, X., Yao, T., Yang, W., Yu, W. and Qu, D.: Co-existence of temperature and amount
10 effects on precipitation $\delta^{18}\text{O}$ in the Asian monsoon region, Geophys. Res. Lett.,
11 38(November), 1–6, doi:10.1029/2011GL049353, 2011.
- 12 Yao, T., Masson-Delmotte, V., Gao, J., Yu, W., Yang, X., Risi, C., Sturm, C., Werner, M.,
13 Zhao, H., He, Y., Ren, W., Tian, L., Shi, C. and Hou, S.: A review of climatic controls on
14 $\delta^{18}\text{O}$ in precipitation over the Tibetan Plateau: Observations and simulations, Rev. Geophys.,
15 51(4), 525–548, doi:10.1002/rog.20023, 2013.
- 16 Zachos, J. C., Dickens, G. R. and Zeebe, R. E.: An early Cenozoic perspective on greenhouse
17 warming and carbon-cycle dynamics., Nature, 451(7176), 279–283, doi:10.1038/nature06588,
18 2008.
- 19 Zhang, R., Jiang, D., Zhang, Z. and Yu, E.: The impact of regional uplift of the Tibetan
20 Plateau on the Asian monsoon climate, Palaeogeogr. Palaeoclimatol. Palaeoecol., 417, 137–
21 150, doi:10.1016/j.palaeo.2014.10.030, 2015.
- 22 Zhang, Z., Wang, H., Guo, Z. and Jiang, D.: What triggers the transition of
23 palaeoenvironmental patterns in China, the Tibetan Plateau uplift or the Paratethys Sea
24 retreat?, Palaeogeogr. Palaeoclimatol. Palaeoecol., 245(3-4), 317–331,
25 doi:10.1016/j.palaeo.2006.08.003, 2007.
- 26 Zhao, Y. and Yu, Z.: Vegetation response to Holocene climate change in East Asian
27 monsoon-margin region, Earth-Science Rev., 113(1-2), 1–10,
28 doi:10.1016/j.earscirev.2012.03.001, 2012.
- 29 Zhisheng, A., Kutzbach, J. E., Prell, W. L. and Porter, S. C.: Evolution of Asian monsoons
30 and phased uplift of the Himalaya-Tibetan plateau since Late Miocene times., Nature,



- 1 411(6833), 62–66, doi:10.1038/35075035, 2001.
- 2 Zhisheng, A., Guoxiong, W., Jianping, L., Youbin, S., Yimin, L., Weijian, Z., Yanjun, C.,
- 3 Anmin, D., Li, L., Jiangyu, M., Hai, C., Zhengguo, S., Liangcheng, T., Hong, Y., Hong, A.,
- 4 Hong, C. and Juan, F.: Global Monsoon Dynamics and Climate Change, *Annu. Rev. Earth*
- 5 *Planet. Sci.*, 43(1), 29–77, doi:10.1146/annurev-earth-060313-054623, 2015.
- 6 Zhuang, G., Brandon, M. T., Pagani, M. and Krishnan, S.: Leaf wax stable isotopes from
- 7 Northern Tibetan Plateau: Implications for uplift and climate since 15 Ma, *Earth Planet. Sci.*
- 8 *Lett.*, 390, 186–198, doi:10.1016/j.epsl.2014.01.003, 2014.
- 9
- 10
- 11
- 12
- 13
- 14
- 15
- 16
- 17
- 18
- 19
- 20
- 21
- 22
- 23
- 24
- 25
- 26



- 1 Table 1. Table detailing how the different terms of the decomposition for ΔR_p , as written in
 2 Eq. (8), are estimated
 3

Term written with differential format	Estimate of these terms	Physical meaning
ΔR_p	$R_p(\delta R_{vi2}, \varepsilon_2, h_2, \delta T_{s2}, z_2)$ $- R_p(\delta R_{vi1}, \varepsilon_1, h_1, \delta T_{s1}, z_1)$	Total isotopic difference between state 1 and state 2
$\frac{\partial R_p}{\partial z} \cdot \Delta z$	$R_p(0,0,1,0, z_2) - R_p(0,0,1,0, z_1)$	Direct effect of topography change
$\frac{\partial R_p}{\partial \delta T_s} \cdot \Delta \delta T_s$	$R_p(0,0,1, \delta T_{s2}, z_2) - R_p(0,0,1, \delta T_{s1}, z_1)$ $-(R_p(0,0,1,0, z_2) - R_p(0,0,1,0, z_1))$	Effect of lapse rate change, associated with non-adiabatic effects, possibly due to changes in surface energy budget or in large-scale atmospheric stratification
$\frac{\partial R_p}{\partial h} \cdot \Delta h$	$R_p(0,0, h_2, \delta T_{s2}, z_2) - R_p(0,0, h_1, \delta T_{s1}, z_1)$ $-(R_p(0,0,1, \delta T_{s2}, z_2) - R_p(0,0,1, \delta T_{s1}, z_1))$	Effect of local relative humidity change, possibly due to large-scale circulation changes
$\frac{\partial R_p}{\partial \varepsilon} \cdot \Delta \varepsilon$	$R_p(0, \varepsilon_2, h_2, \delta T_{s2}, z_2)$ $- R_p(0, \varepsilon_1, h_1, \delta T_{s1}, z_1)$ $-(R_p(0,0, h_2, \delta T_{s2}, z_2)$ $- R_p(0,0, h_1, \delta T_{s1}, z_1))$	Effect of changes in condensational and post-condensational effects, possibly due to changes in rain reevaporation processes
$\frac{\partial R_p}{\partial R_{vi}} \cdot \Delta \delta R_{vi}$	$R_p(\delta R_{vi2}, \varepsilon_2, h_2, \delta T_{s2}, z_2)$ $- R_p(\delta R_{vi1}, \varepsilon_1, h_1, \delta T_{s1}, z_1)$	All other effects, including effects of deep convection, mixing, water vapor origin,



$$-(R_p(0, \varepsilon_2, h_2, \delta T_{s2}, z_2)$$

continental recycling on

$$- R_p(0, \varepsilon_1, h_1, \delta T_{s1}, z_1))$$

the initial water vapor

1

2

3

4

5

6

7

8

9

10

11

12

13

14

15

16

17

18

19

20

21

22

23



1 Table 2. Values of isotopic changes due to decomposed terms for two uplift stages and for
 2 two regions (see the text)

Term	Isotopic change (‰)			
	Initial Stage		Terminal Stage	
	South	North	South	North
$\frac{\partial R_p}{\partial z} \cdot \Delta z$	-1.40	-2.00	-3.96	-5.50
$\frac{\partial R_p}{\partial \delta T_s} \cdot \Delta \delta T_s$	0.4	-0.09	0.76	-0.25
$\frac{\partial R_p}{\partial h} \cdot \Delta h$	2.40	1.97	1.38	2.50
$\frac{\partial R_p}{\partial \varepsilon} \cdot \Delta \varepsilon$	-1.30	-1.73	-0.41	0.01
$\frac{\partial R_p}{\partial R_{vi}} \cdot \Delta \delta R_{vi}$	-1.10	-0.14	-2.38	-0.54
Total ΔR_p	-1.00	-1.99	-4.61	-3.16

3

4

5

6

7

8

9

10

11

12

13



1

2 Table 3. Impact of the different terms of the decomposition on the isotopic signal for the
 3 terminal stage of HTP uplift in the location where paleoelevation studies have been done

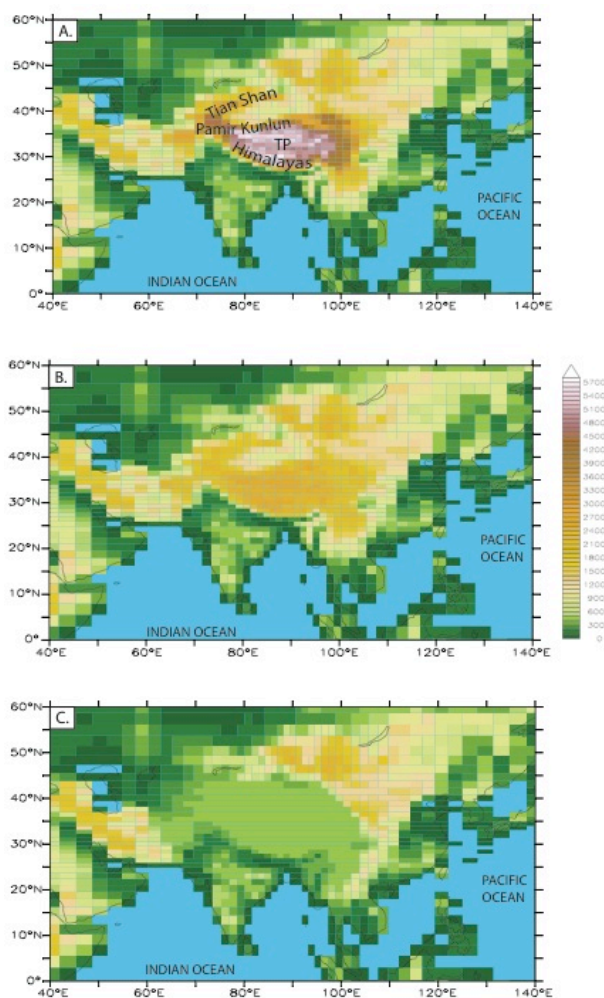
Locality	Latitude	Longitude	ΔR_p (‰)	$\frac{\partial R_p}{\partial z} \cdot \Delta z$ (‰)	$\frac{\partial R_p}{\partial \delta T_s} \cdot \Delta \delta T_s$ (‰)	$\frac{\partial R_p}{\partial \varepsilon} \cdot \Delta \varepsilon$ (‰)	$\frac{\partial R_p}{\partial h} \cdot \Delta h$ (‰)	$\frac{\partial R_p}{\partial R_{vi}} \cdot \Delta \delta R_{vi}$ (‰)	Paleoelevation studies at this locality
Aertashi	37.97	75.55	-1.619	-2.859	0.9986	-0.2935	-0.2679	0.8033	Kent-Corson et al. (2009)
Biger Noor	45.90	96.78	-1.169	-0.004360	2.673	-0.7024	-4.419	1.283	Caves et al. (2014)
Chake Basin	23.80	103.10	-0.2520	0.006192	-0.03002	0.04205	0.2631	-0.5333	Hoke et al. (2014)
Dzereg	47.14	93.06	-1.006	-0.003550	2.216	-0.3723	-4.313	1.466	Caves et al. (2014)
Eryuan	26.20	99.80	-1.356	-1.574	0.6337	0.1705	0.4971	-1.083	Hoke et al. (2014)
Ganchaigou	37.69	91.04	-3.195	-2.780	0.8363	-1.292	0.6104	-0.5692	Kent-Corson et al. (2009)
Gyirong Basin	28.70	85.25	-7.017	-3.850	1.073	-1.089	0.4085	-3.559	Wang et al. (1996)
Hexi Corridor	39.52	97.52	-2.907	-0.2788	1.732	-1.985	-2.293	-0.08312	Kent-Corson et al. (2009)
HohXil Basin	34.60	93.00	-3.972	-6.529	0.6597	0.03659	3.375	-1.514	Cyr et al. (2005)
Huaitoutala	37.30	96.70	-5.998	-4.418	-1.473	-3.620	3.104	0.4089	Zhuang et al. (2011)
India Siwaliks	30.35	77.60	-1.862	0.005774	0.1029	-0.3033	0.1828	-1.851	Ghosh et al. (2004)
India Siwaliks	30.34	77.60	-1.862	0.005774	0.1029	-0.3033	0.1828	-1.851	Sanyal et al. (2005)
Janggalsay	38.15	86.62	-4.487	-2.406	1.026	-2.347	-0.9517	0.1923	Kent-Corson et al. (2009)



Jianchuan Basin	26.60	99.80	-1.356	-1.574	0.6337	0.1705	0.4971	-1.083	Hoke et al. (2014)
Jingou	44.75	85.40	1.073	-0.03134	1.270	1.435	-2.054	0.4526	Charreau et al. (2012)
Kailas Basin	31.20	81.00	-6.705	-7.181	0.4011	0.7988	3.162	-3.886	DeCelles et al. (2011)
Kuitun	45.00	84.75	1.073	-0.03134	1.270	1.435	-2.054	0.4526	Charreau et al. (2012)
Lake Mahai	37.66	94.24	-0.9639	-0.002379	2.737	0.4231	-4.188	0.06643	Kent-Corson et al. (2009)
Lanping	26.50	99.40	-1.356	-1.574	0.6337	0.1705	0.4971	-1.083	Hoke et al. (2014)
Lao Mangnai	36.94	91.96	-1.133	-3.998	0.4470	0.3556	2.233	-0.1708	Kent-Corson et al. (2009)
Lenghu	37.84	93.36	-0.9639	-0.002379	2.737	0.4231	-4.188	0.06643	Kent-Corson et al. (2009)
Linxia Basin	35.69	103.10	0.4433	-0.9613	1.079	0.3638	-0.4095	0.3712	Dettman et al. (2003)
Linzhou Basin	30.00	91.20	-6.756	-5.956	2.337	0.05738	0.8857	-3.965	Ding et al. (2014)
Luhe	25.20	101.30	-0.2417	0.008419	0.3172	0.4105	-0.2359	-0.7419	Hoke et al. (2014)
Lulehe	37.50	95.08	0.06084	-0.9874	1.724	1.950	-3.326	0.5784	Kent-Corson et al. (2009)
Lulehe	37.50	95.08	0.06084	-0.9874	1.724	1.950	-3.326	0.5784	Kent-Corson et al. (2009)
Lunpola Basin	32.06	89.75	-6.763	-6.073	1.920	-0.6516	1.561	-3.520	Rowley and Currie (2006)
Miran River	38.98	88.85	-4.786	-1.387	1.069	-2.683	-2.068	0.2831	Kent-Corson et al. (2009)
Nepal Siwaliks	27.42	82.84	-1.370	0.006081	-0.01583	0.2030	0.02450	-1.588	Quade et al. (1995)
Nima Basin	31.75	87.50	-5.897	-7.724	-0.2050	1.312	4.078	-3.359	DeCelles et al.



									al. (2011)
Oiyug Basin	29.70	89.50	-10.39	-7.842	2.634	-2.598	1.151	-3.735	Currie et al. (2005)
Oytag	38.98	75.51	-0.4993	-0.7157	1.320	0.7194	-1.975	0.1524	Bershaw et al. (2011)
Pakistan									Quade et al. (1995)
Siwaliks	33.39	73.11	0.6450	0.007831	0.3801	0.4070	0.3792	-0.5291	
Puska	37.12	78.60	-2.598	0.006383	0.8959	-0.4719	-3.909	0.8806	Kent-Corson et al. (2009)
Taatsin Gol	45.42	101.26	-0.7307	-0.002622	1.600	-0.3638	-3.087	1.123	Caves et al. (2014)
Thakkhola	28.70	83.50	-4.018	-1.529	0.8024	-0.3101	-0.5717	-2.409	Garzione et al. (2000)
Thakkhola-Tetang	28.66	83.50	-4.018	-1.529	0.8024	-0.3101	-0.5717	-2.409	Garzione et al. (2000)
Xiao Qaidam	37.03	94.88	1.614	-1.376	1.772	3.117	-2.581	0.6811	Kent-Corson et al. (2009)
Xifeng	35.70	107.60	0.2447	0.00	0.5220	0.1725	-0.009882	-0.4401	Jiang et al. (2002)
Xorkol	39.01	91.92	-3.218	-0.8709	1.871	-1.302	-2.970	0.05405	Kent-Corson et al. (2009)
Xunhua Basin	35.90	102.50	0.4433	-0.9613	1.079	0.3638	-0.4095	0.3712	Hough et al. (2010)
Yanyuan	27.50	101.50	-0.3498	-1.152	0.6572	0.5390	0.3733	-0.7672	Hoke et al. (2014)
Zhada Basin	31.50	79.75	-3.983	-4.818	-0.04606	0.8307	2.708	-2.657	Saylor et al. (2009)



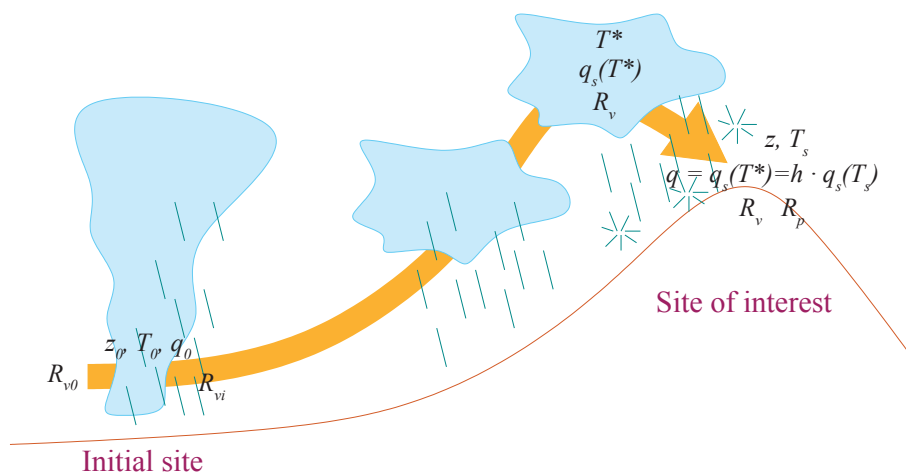
1

2

3 Figure 1. Models design (A) 100% of modern topography - MOD case; (B) Tibetan Plateau,
4 Himalayas, Tian Shan, Pamir, Kunlun and Hindu Kush elevations reduced to 50% of modern
5 elevation - INT case; (C) Tibetan Plateau, Himalayas, Tian Shan, Pamir, Kunlun and Hindu
6 Kush elevations reduced to 250 m - LOW case. Black rectangles show the division of the TP
7 by regions: southern TP (between 25°N and 30°N), central TP (between 30°N and 35°N) and
8 northern TP (between 35°N and 40°N).

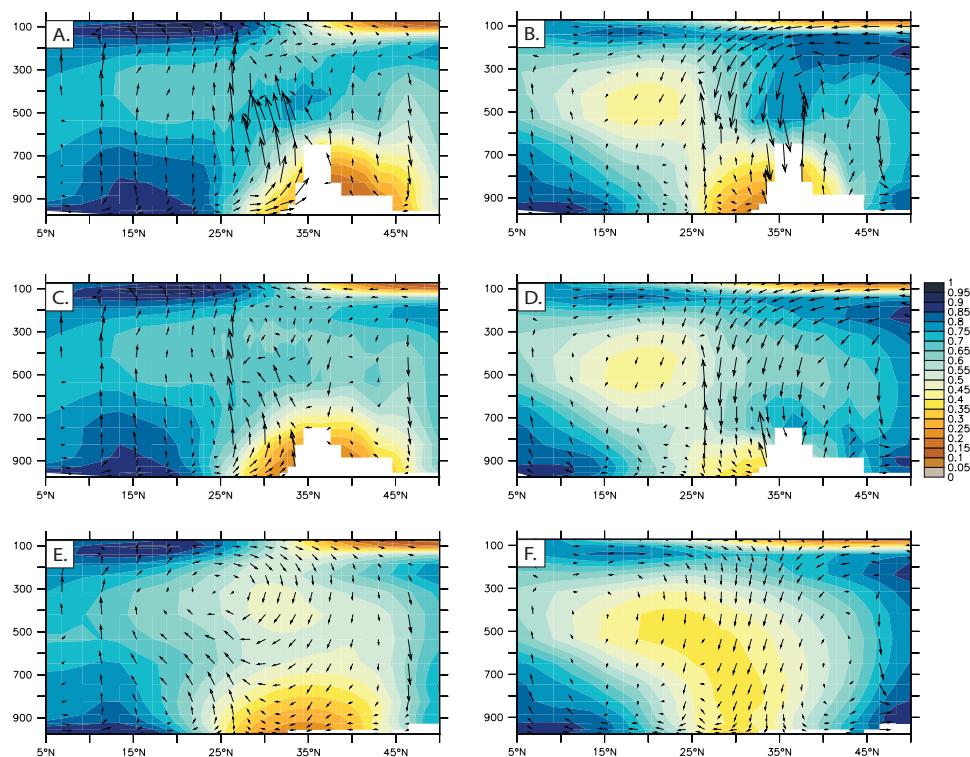
9

10



1
 2
 3
 4
 5
 6
 7
 8
 9
 10
 11
 12
 13
 14
 15
 16
 17
 18

Figure 2. Idealized framework of an isolated air parcel transported from an initial site at low altitude to the site of interest. Most notations are illustrated.



1

2

3 Figure 3. Cross-TP profiles (averaged between 70 and 90°E) showing the relative humidity
4 and moisture transport for seasons (A, C, E) MJJAS and (B, D, F) ONDJFMA and for 3
5 simulation: (A, B) MOD, (C, D) INT, (E, F) LOW cases.

6

7

8

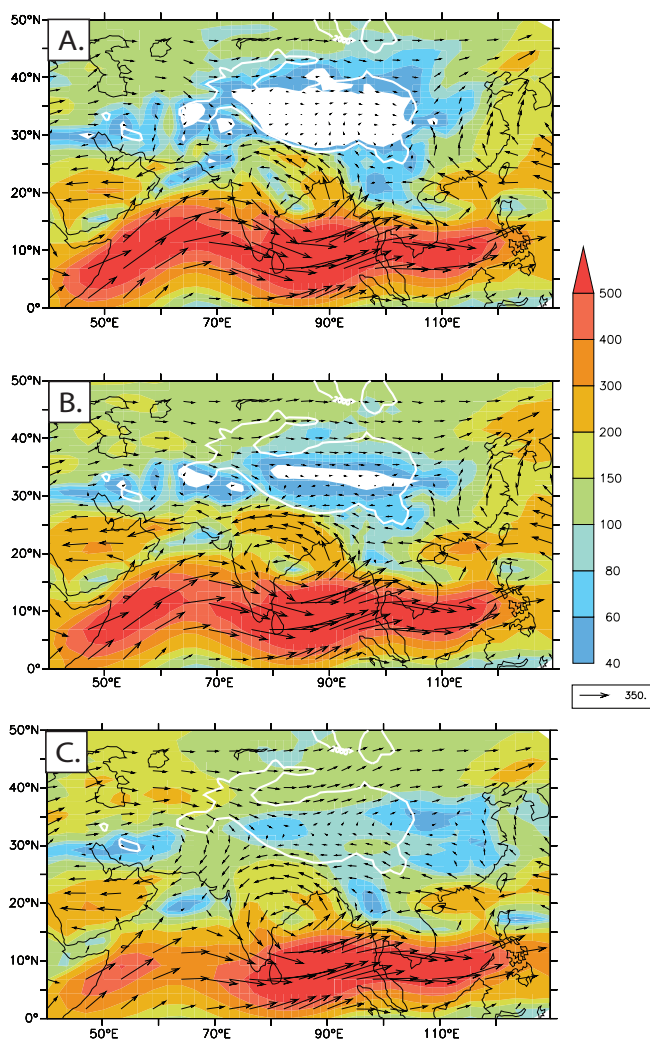
9

10

11

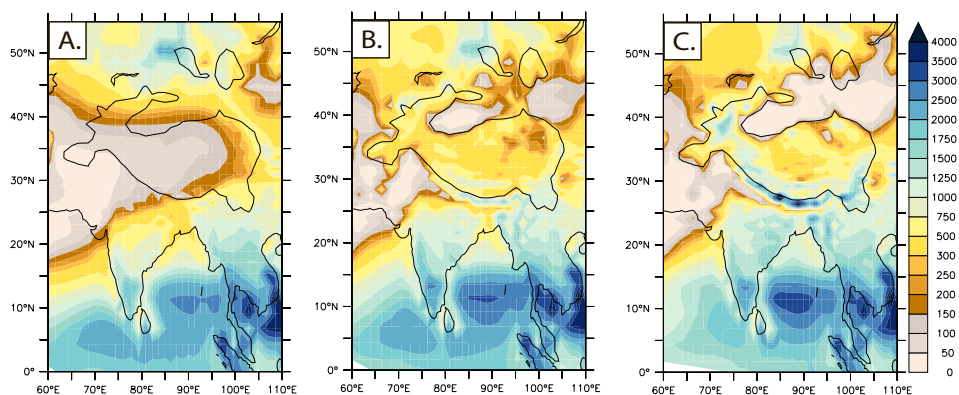
12

13



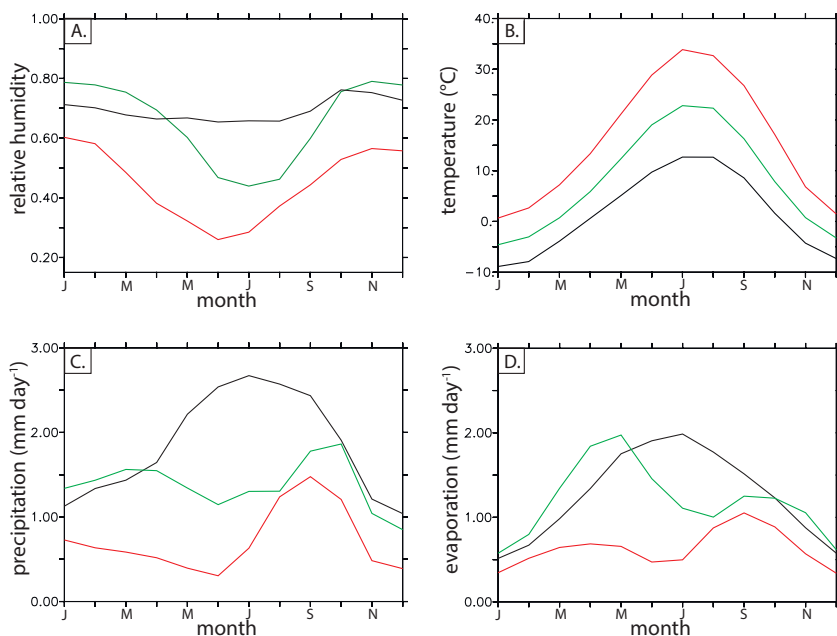
1
2
3
4
5
6
7
8

Figure 4. Directions and intensity of JJA vertically-integrated humidity transport for: (A) MOD case, (B) INT case, (C) LOW case.



1
2
3
4
5
6
7
8
9
10
11
12
13
14
15
16
17
18
19

Figure 5. Annual mean precipitation amount (absolute values, mm/year) for: (A) LOW case, (B) INT case, (C) MOD case.



1

2

3 Figure 6. Intraannual variations in (A) low level relative humidity, (B) near-surface
4 temperature, (C) precipitation amount and (D) evaporation amount. All variables are averaged
5 for TP with the altitude over 1500 m. Black colour corresponds to MOD experiment, green -
6 for INT experiment and red - for LOW experiment.

7

8

9

10

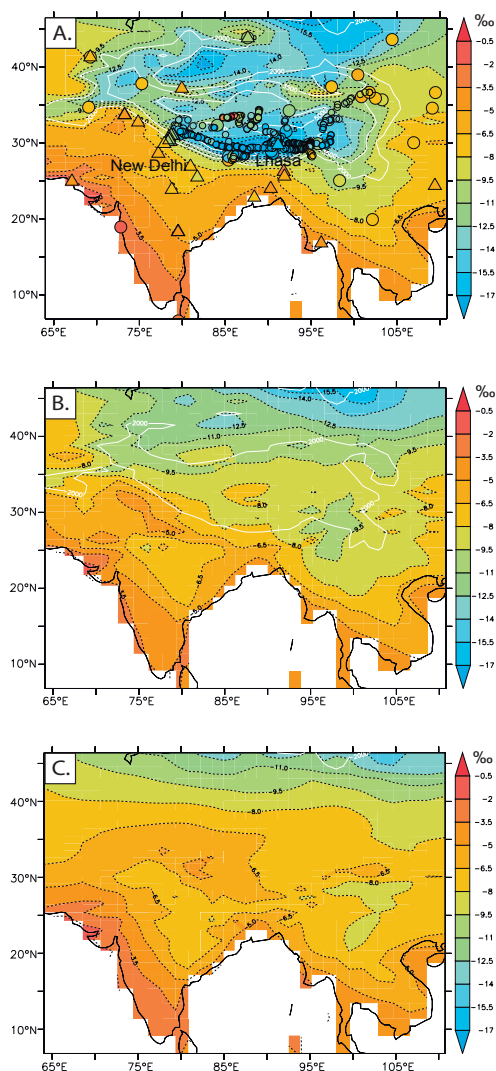
11

12

13

14

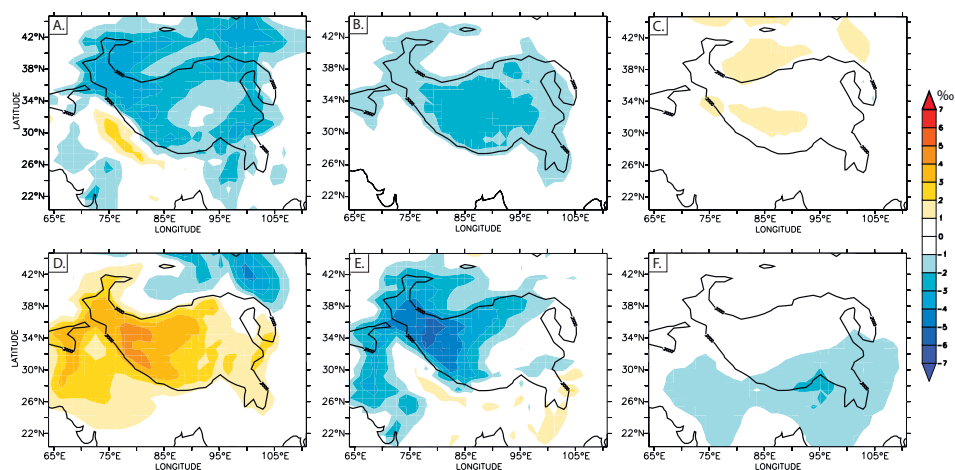
15



1

2

3 Figure 7. Annual mean $\delta^{18}\text{O}$ in precipitation simulated by LMDZ-iso for: (A) MOD case, (B)
4 INT case, (C) LOW case. Triangles show $\delta^{18}\text{O}$ in precipitation from GNIP stations, big circles
5 – $\delta^{18}\text{O}$ in precipitation from Caves et al. (2015) compilation (annual mean and JJA values
6 respectively), small circles represent $\delta^{18}\text{O}$ in streams, lakes and springs compiled from Quade
7 et al., 2011, Bershaw et al., 2012, Hren et al., 2009



1

2

3 Figure 8. (A) Total isotopic difference between INT and LOW experiments (ΔR_p) and spatial
 4 isotopic variations related to: (B) direct effect of topography changes, (C) effect of lapse rate
 5 change, associated with non-adiabatic effects, (D) effect of local relative humidity change, (E)
 6 effect of changes in post-condensational processes, (F) all other effect (see Table 1)

7

8

9

10

11

12

13

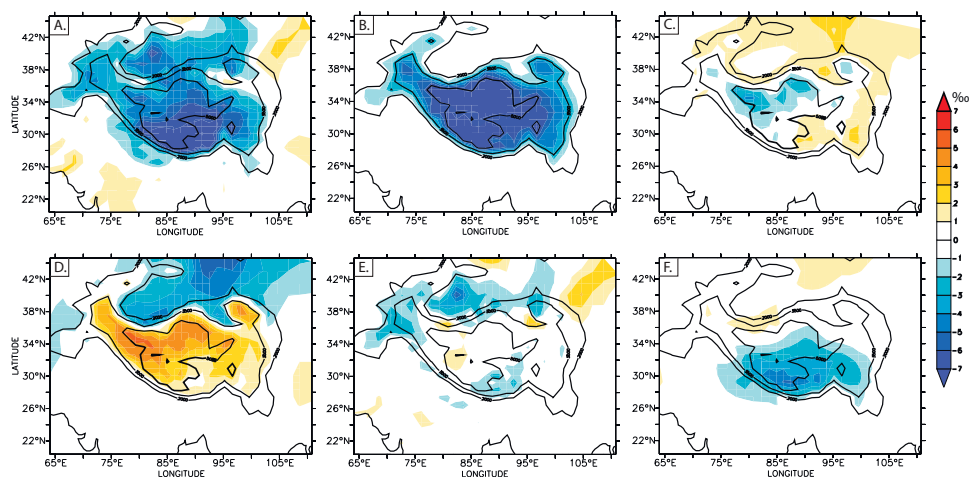
14

15

16

17

18



1

2

3 Figure 9. (A) Total isotopic difference between MOD and INT experiments (ΔR_p) and spatial
 4 isotopic variations related to: (B) direct effect of topography changes, (C) effect of lapse rate
 5 change, associated with non-adiabatic effects, (D) effect of local relative humidity change, (E)
 6 effect of changes in post-condensational processes, (F) all other effect (see Table 1)

7

8

9

10

11

12

13

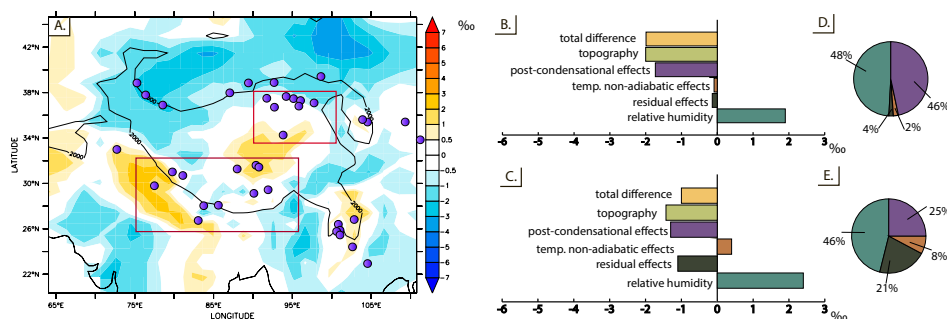
14

15

16

17

18



1

2

3 Figure 10. Difference in $\delta^{18}\text{O}_p$ between INT and LOW experiments that is not related to direct
4 effect of topography changes. Violet points show Cenozoic paleoelevation studies locations
5 (compiled from Caves et al., 2015). Red rectangles show regions for that averaged values
6 decomposed terms are shown: B) Northern region, C) Southern region. Pie diagrams show
7 portion of total isotopic difference related to processes other than topography: D) Northern
8 region, E) Southern region

9

10

11

12

13

14

15

16

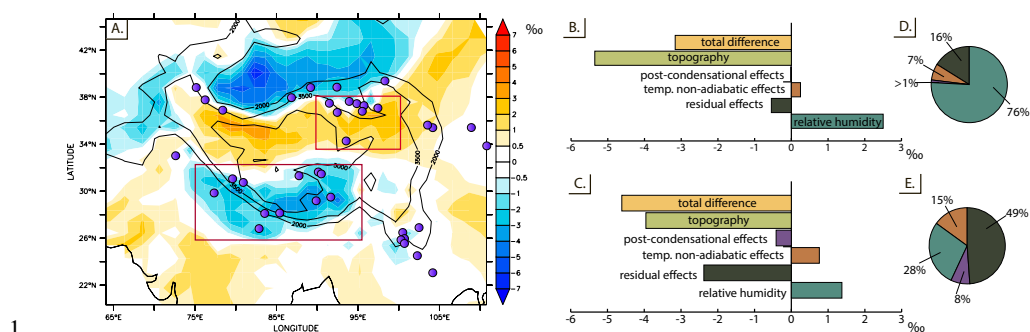
17

18

19

20

21



1

2

3 Figure 11. Difference in $\delta^{18}O_p$ between MOD and INT experiments that is not related to direct
4 effect of topography changes. Violet points show Cenozoic paleoelevation studies locations
5 (compiled from Caves et al., 2015). Red rectangles show regions for that averaged values
6 decomposed terms are shown: B) Northern region, C) Southern region. Pie diagrams show
7 portion of total isotopic difference related to processes other than topography: D) Northern
8 region, E) Southern region.

9

10

11

12

13

14

15

16

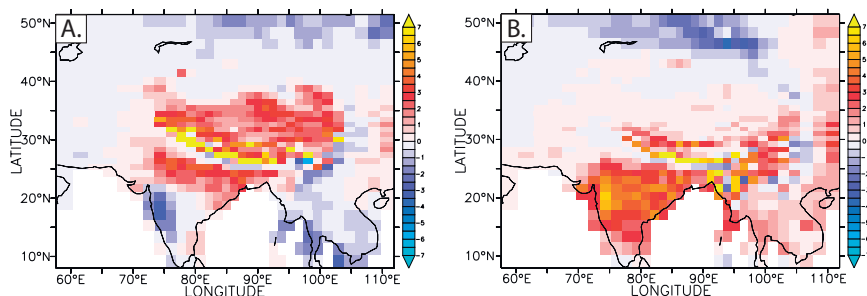
17

18

19

20

21



1
2
3
4
5
6
7

Figure 12. Precipitation change for A) MOD-INT B) INT-LOW cases